Temperature dependence of exciton and charge carrier dynamics in organic thin films

A. D. Platt, M. J. Kendrick, M. Loth, J. E. Anthony, and O. Ostroverkhova

Phys. Rev. B **84**, 235209 — Published 22 December 2011

DOI: 10.1103/PhysRevB.84.235209

Temperature dependence of exciton and charge carrier dynamics in organic thin films

A.D. Platt,[1**] M. J. Kendrick,[1**] M. Loth,[2] J. E. Anthony,[2] and O. Ostroverkhova[1*]

[1] Department of Physics, Oregon State University, Corvallis, OR 97331

[2] Department of Chemistry, University of Kentucky, Lexington, KY

*Corresponding author: electronic mail oksana@science.oregonstate.edu

**These authors contributed equally

Abstract

We report on physical mechanisms behind the temperature-dependent optical absorption, photoluminescence (PL), and photoconductivity in spin-coated films of a functionalized anthradithiophene (ADT) derivative, ADT-TES-F, and its composites with C_{60} and another ADT derivative, ADT-TIPS-CN. Measurements of absorption and PL spectra, PL lifetimes, and transient photocurrent were performed at temperatures between 98 K and 300 K as a function of applied electric field. In pristine ADT-TES-F films, absorptive and emissive species were identified to be disordered H-aggregates whose properties are affected by static and dynamic disorder. The exciton bandwidths were ≤0.06 eV and ~0.115 eV for absorptive and emissive aggregates, respectively, indicative of higher disorder in the emissive species. The exciton in the latter was found to be delocalized over ~4-5 molecules. The PL properties were significantly modified upon adding a guest molecule to the ADT-TES-F host. In ADT-TES-F/C_{60} composites, the PL was

considerably quenched due to photoinduced electron transfer from ADT-TES-F to C_{60}, while in ADT-TES-F/ADT-TIPS-CN blends, the PL was dominated by emission from an exciplex formed between ADT-TES-F and ADT-TIPS-CN molecules. In all materials, PL quantum yield dramatically decreased as the temperature increased due to thermally activated nonradiative recombination. Considerable electric-field-induced PL quenching was observed at low temperatures at electric fields above ~10^5 V/cm due to tunneling into dark states. No significant contribution of ADT-TES-F emissive exciton dissociation to transient photocurrent was observed.

In all materials, charge carriers were photogenerated at sub-500 ps time scales, limited by the laser pulse width, with temperature- and electric field-independent photogeneration efficiency. In ADT-TES-F/C_{60} (2%) composites, the photogeneration efficiency was a factor of 2-3 higher than that in pristine ADT-TES-F films. In ADT-TES-F/ADT-TIPS-CN (2%) blends, an additional charge carrier photogeneration component was observed at room temperature at time scales of ~20 ns due to exciplex dissociation. At ~0.5-5 ns after photoexcitation, the carriers propagated via thermally- and electric field-activated hopping with an activation energy of ~0.025 eV. At time scales longer than ~5 ns, charge transport of carriers that are not frozen in traps proceeded through tunneling via isoenergetic sites.

I. INTRODUCTION

Organic (opto)electronic materials are of interest due to their low cost and tunable properties.[1] Solution processable materials that can be cast into thin films using various solution deposition techniques are especially advantageous.[2] Additionally, such materials can be used to create a variety of composites with properties tailored for specific applications. Functionalized anthradithiophene (ADT) derivatives have attracted attention due to their high charge carrier (hole) mobilities (e.g. >1.5 $cm^2/(Vs)$[3,4] in spin-coated thin films of the fluorinated ADT derivative functionalized with triethylsilylethynyl (TES) side groups, ADT-TES-F in Fig.1(a)), fast charge carrier photogeneration, high photoconductive gain, and relatively strong photoluminescence (PL) in solution-deposited thin films.[5-9] Some of these properties of ADT derivatives have been exploited in thin-film transistors (TFTs)[3,4,10-12] and solar cells;[13,14] additionally, ADTs are promising for applications in photodetectors,[5,15] light-emitting diodes,[16] and lasers.[17] ADT-TES-F molecules form two-dimensional (2D) π-stacked arrangements with short interplanar spacings of 3.2-3.4 Å, favoring high charge carrier mobility, and pack into a triclinic crystal structure with space group $P\bar{1}$.[4,10-12,18] Structure and morphology dependence of solution-deposited crystalline ADT-TES-F films based on the film deposition methods, on the choice of the substrate and its treatment, and on the device geometry have been extensively studied and related to ADT-TES-F TFT characteristics.[4,11,12] In addition, it has been previously demonstrated on various ADT films that the optical absorption, PL, and photoconductive properties depend significantly on the molecular packing and intermolecular interactions.[5,8,9] However, physical mechanisms which enable promising (opto)electronic properties of ADT derivatives are

not completely understood and need to be established to aid in the design of new-generation functionalized derivatives with improved performance. One of the goals of this paper is to gain insight into these physical mechanisms by thoroughly analyzing the temperature dependence of optical absorption, PL and photoconductive properties of ADT-TES-F films.

A promising venue for designing materials with optoelectronic properties fine-tuned for a particular application is creating composites with specific charge and energy transfer properties. Optoelectronic properties of solution-deposited thin films of ADT-based composites have been previously investigated, and effects of guest-host interactions on exciton and charge carrier dynamics were observed.[7-9] Depending on the guest molecule introduced in the ADT-TES-F host, the photoexcited charge carrier dynamics could be dramatically varied, depending on the efficiency of the photoinduced charge transfer between guest and host molecules. These earlier studies identified complex interactions contributing to optoelectronic properties of these composites, which are still not well understood and will be further investigated here. For the present study of ADT-TES-F-based guest-host composites, we chose C_{60} and another ADT derivative, ADT-TIPS-CN (Fig.1(a)), as guest molecules. The choice was governed by our previous knowledge of the photoinduced electron transfer from ADT-TES-F to C_{60}[7] and of the exciplex formation between ADT-TES-F and ADT-TIPS-CN.[9] Thus, the chosen composites serve as model systems for physical studies of the effects of complete and partial charge transfer processes, respectively, on exciton and charge carrier dynamics in ADT-TES-F-based films.

In this paper, we present a detailed study of the physical mechanisms that determine optical absorption, PL, and photoconductive properties of ADT-TES-F films and guest-host composite films with ADT-TES-F as the host. In particular, we seek to understand: 1) intermolecular interactions that determine optical absorption and PL properties; 2) the origin and mechanism of fast charge photogeneration; 3) the mechanism of charge transport, and 4) the role of static and dynamic disorder in absorption, PL, and charge transport. Specific questions to be addressed include: (i) how does molecular 2D π-stacking contribute to optical absorption (Sec. III.A.1) and PL emission (Sec. III.A.2); (ii) does charge photogeneration rely on dissociation of the emissive exciton (Sec. III.A.3 and III.A.4); (iii) what is the role of guest-host charge transfer in charge photogeneration and PL emission (Sec. III.B and III.C); (iv) is charge transport bandlike or hopping (Sec.III.A.4); and (v) what is the origin of disorder contributing to optical absorption, PL emission and charge transport (Sec.IV)?

In order to establish physical mechanisms outlined above, we performed a study of the temperature and electric field dependence of the optical absorption and PL spectra, PL lifetimes, and transient photocurrent in films of pristine ADT-TES-F and its composites; from which we sought a physical model that would be consistent with all experimental observations. The paper is organized as follows. Section II describes sample preparation, characterization of film structure and morphology, and experimental methods. Section III presents analysis of optical absorption, PL, and photoconductive properties of pristine ADT-TES-F films (Sec. III.A), ADT-TES-F/C_{60} composite films (Sec. III.B), and ADT-TES-F/ADT-TIPS-CN composite films (Sec. III.C), at various temperatures. Section IV further discusses results and presents a physical picture of exciton and photoinduced

charge carrier dynamics in ADT thin films that supports the observations of Section III. Section V summarizes the findings of the paper.

II. EXPERIMENTAL DETAILS

A. Materials and sample preparation

The materials used in our studies are the ADT-TES-F derivative, an ADT derivative containing cyano end groups and triisopropylsilylethynyl (TIPS) side groups, ADT-TIPS-CN (Fig.1(a)), and C_{60}.[5,7,9] The highest occupied and lowest unoccupied molecular orbital (HOMO and LUMO, respectively) energies of ADT-TES-F and ADT-TIPS-CN measured using differential pulse voltammetry[5] are shown in Fig.1(b). The HOMO and LUMO levels of C_{60}, taken from Ref.19, are also included.

For preparation of pristine ADT-TES-F films, a 2×10^{-2} M toluene solution was used. For ADT-TES-F/ADT-TIPS-CN blends, a composite solution of ADT-TES-F (98 wt%) with ADT-TIPS-CN (2 wt%) in toluene was prepared from stock solutions of 2×10^{-2} M ADT-TES-F and 10^{-3} M ADT-TIPS-CN. For similar wt/wt ratio ADT-TES-F/C_{60} films, a composite solution of ADT-TES-F (98 wt%) with C_{60} (2 wt%) was prepared from stock solutions of 2×10^{-2} M and 3.5×10^{-3} M, respectively. Solutions were spin-coated at 4000 rpm onto glass substrates with photolithographically deposited 5 nm/50 nm thick Cr/Au interdigitated electrode pairs. Electrodes consisted of 10 pairs of 1 mm long fingers with 25 μm finger width and 25 μm gaps (L) between the fingers of opposite electrodes.

This preparation method resulted in polycrystalline films, as confirmed by x-ray diffraction (XRD), with an average grain size of several microns (atomic force microscopy images are included in the Supporting Information).[20] The ADT-TES-F

single crystal has a triclinic structure with unit cell parameters a = 7.21 Å (7.12 Å), b = 7.32 Å (7.23 Å), c = 16.35 Å (16.63 Å), α = 87.72° (97.52°), β = 89.99° (91.36°), γ = 71.94° (107.49°) at temperatures above (below) 294 K, with a solid-solid phase transition occurring at 294 K. [4,11,12,18] XRD data from our films (included in the Supporting Information)[20] exhibited peaks corresponding to (00l) (l =1,3,4) orientations, indicative of an ordered molecular structure with a vertical intermolecular spacing of 16.6 Å;[3] on untreated glass substrates such as those used in our studies, the in-plane orientation of the crystallites is random.[12] The (001) crystal orientation, predominant in ADT-TES-F films, corresponds to the molecular π-planes and the long axis of the conjugated core oriented approximately in the plane of the film,[12] which enables efficient charge transport in TFTs. However, detailed 2D grazing incidence XRD measurements on ADT-TES-F films on untreated glass substrates[12] also revealed the presence of crystallites with (111) orientations, in which π-planes are parallel to the film surface, detrimental for in-plane charge transport. Such crystallites introduce additional disorder and lower the overall charge carrier mobility (Sec. IV).[21]

For our temperature dependence studies, the samples were placed in a custom built fixture, mounted in an optical cryostat (liquid nitrogen; sample in vacuum), and photoexcited from the substrate side. The temperature was varied between 300 K and 98 K, and measurements of optical absorption spectra, PL spectra and lifetimes, and transient photocurrent were performed *in situ*. Selected measurements were performed in the extended temperature range between 355 K and 98 K.

B. Measurements of optical and PL properties

The absorption spectra were measured using the Ocean Optics USB4000 spectrometer and a halogen white light source (3100 K blackbody). The lamp was fiber delivered to a collimating lens focused on the active region of the sample and some of the surrounding area (~2 mm diameter). Light transmitted through the sample was collected through a second collimating lens and coupled by fiber to the spectrometer. For the reference signals, the cryostat was translated so as to illuminate an empty region (free of the film and of electrodes) on the glass substrate.

The PL was excited with a 355 nm frequency-tripled Nd:YAG laser, using excitation conditions similar to those utilized in the photocurrent measurements (Sec. II.C), and detected with another fiber coupled spectrometer (Ocean Optics USB2000) calibrated against a 3100 K blackbody emitter. (The independence of the PL spectra in ADT derivatives on the excitation wavelength at wavelengths above the absorption edge has been previously verified.)[5]

PL lifetime measurements were taken under 400 nm excitation from a frequency-doubled 80 fs Ti:Sapphire laser with a repetition rate of 93 MHz picked at 9.3 MHz using a custom-built pulse picker (based on a TeO_2 acousto-optic modulator from Neos, Inc.).[5,8,9] A time-correlated single photon counter (TCSPC) board (PicoQuant TimeHarp 200) was used with a single photon avalanche photodiode (SPAD – Molecular Photonic Devices) for detection. Combinations of various filters including 3RD440LP (Omega Optical), CG475LP (CVI), HQ535LP, HQ610SP, E625SP, D680/80x, and D740/80x (all from Chroma Tech.) were used to study PL lifetimes of various spectral regions within the PL

emission spectra. The instrument response function (IRF) (~ 200 ps) was recorded using scattered light from an etched microscope slide.

For measurements of electric field dependence of optical absorption, PL spectra, and PL lifetimes, voltage was applied to samples using a Keithley 237 source-measure unit, and the measurements described above were performed as a function of applied voltage (0-600 V).

C. Measurements of photocurrent

For transient photocurrent measurements, a 355 nm 500 ps 0.4 μJ/cm^2 pulsed excitation (cavity Q-switched Nd:YAG laser, 44.6 kHz, from Nanolase) source was used. Voltage (V) was applied to the samples using a Keithley 237 source-measure unit, and the transient photocurrent was measured using either a 50 GHz digital sampling oscilloscope (CSA8200/Tek80E01) or Agilent DSO6032A.[5-7,22] The time resolution was about 500 ps, limited by the laser pulse width. The average applied electric field (E) was calculated using $E = V/L$, where L is the gap between the electrodes.

III. RESULTS

A. Pristine ADT-TES-F films

In Sections III.A.1 and III.A.2, we will establish contributions of intermolecular interactions between π-stacked molecules, as well as static and dynamic disorder, to optical absorption and PL properties of pristine ADT-TES-F films. Also in Section III.A.2, time-resolved exciton dynamics and mechanisms of nonradiative recombination

will be explored. In Section III.A.3, electric field-induced dissociation of the emissive excitons will be investigated. In Section III.A.4, dependence of the transient photocurrent on the electric field and temperature will be analyzed to determine charge transport mechanism and effects of disorder on charge transport. Additionally, results of Sections III.A.3 and III.A.4 will be compared to investigate the origin of photogenerated charge carriers.

1. Optical absorption

Optical absorption spectra of various ADT derivatives in solution and in drop cast films in the temperature range of 278-353 K have been discussed in Ref.5. Spectra of isolated ADT-TES-F molecules (either in solution or in a solid matrix such as PMMA) exhibit exciton coupling to a vibrational mode with an effective wave number ω_{eff} of ~1400 cm^{-1} (0.173 eV), characterized by the Huang-Rhys factor *S* of 0.6 and a Gaussian width σ_{abs} of the 0-0 line of about 235 cm^{-1} (0.029 eV).[5,8,9,23-25] Spin-coated ADT-TES-F films prepared as described in Section II.A exhibited absorption spectra shown in Fig.2(a). (The position of the absorption maximum, corresponding to the $S_0 \rightarrow S_1$ 0-0 transition in a dilute ADT-TES-F solution in toluene[5] is also included in the figure.) The spectra converted into energy units were fit with multiple Gaussians $((I_i/(\sigma_i\sqrt{2\pi}))\exp(-(\omega-\omega_i)^2/2\sigma_i^2))$ to obtain peak areas I_i, positions ω_i, and Gaussian widths σ_i.[9,26] At 298 K (room temperature), a red-shift of the film spectrum with respect to that of isolated ADT-TES-F molecules, $D \approx 870$ cm^{-1} (~0.108 eV) in Fig.2(a), was observed and attributed to enhanced Coulomb interaction of the molecule with its surrounding environment and exchange interactions between translationally equivalent molecules.[5,27-30] Similar to the

ADT-TES-F isolated molecule spectrum,[5] vibronic progression was observed in the film spectra,[5,8,12,26,31] which could be described as exciton coupling to an intramolecular vibrational mode with an effective wave number ω_{eff} of ~1360 cm^{-1} (0.168 eV) at all temperatures.[32-35] Peak positions of the lowest-energy absorption bands A_1 and A_2 as a function of temperature are shown in Fig.2(b), along with linear fits describing their evolution with the temperature. The fits yielded slopes of $(2.0\pm0.2)\times10^{-4}$ eV/K and $(2.2\pm0.4)\times10^{-4}$ eV/K and intercepts of 2.182±0.005 eV and 2.350±0.009 eV for the bands A_1 and A_2, respectively. The red-shift of the absorption spectra upon the temperature decrease has been reported in various organic films[26,34,36] and attributed to freezing out of the torsional and librational modes, which promotes exciton delocalization, as well as to a thermal contraction of the lattice leading to an increase in nonresonant intermolecular interactions (which would increase the parameter *D* in Fig.2(a)).[30] In ADT-TES-F films, these effects were relatively strong, as the peak red-shift rate of $\sim2\times10^{-4}$ eV/K in ADT-TES-F films was a factor of ~2-5 higher than that in, for example, conjugated polymers[26] and PTCDA crystals.[34] Absorption peaks in the film spectra were broadened as compared to those in solution, at all temperatures studied. For example at 298 K, the Gaussian width σ_{abs} of the A_1 band was ~450 cm^{-1} (0.056 eV), a factor of ~2 larger than that of the 0-0 absorption peak in solution.[5] As the temperature decreased, σ_{abs} slightly decreased (Fig.2), reaching a value of ~370 cm^{-1} (0.046 eV) at 100 K (for the A_1 band). This suggests that line broadening in the absorption spectrum of ADT-TES-F films in the studied temperature range is dominated by a weakly temperature-dependent static disorder, which has a considerable contribution from solid-state defects such as

dislocations and grain boundaries.[12] At all temperatures, an intermediate disorder regime, at which $\sigma_{abs} \leq S\omega_{eff} \approx 0.1$ eV,[37] was maintained.

As the temperature decreased, the ratio of the peak amplitudes of the bands A_1 and A_2 increased from 1.25 at 298 K to 1.56 at 100 K, approaching a value of ~1.66 observed in the spectra of isolated ADT-TES-F molecules. From these observations, we sought a model describing this behavior. Given the π-stacking properties of ADT-TES-F molecules,[10,12] signatures of H (cofacial)-aggregate formation would be expected in spectra of ADT-TES-F films.[29] This prompted our analysis of the ADT-TES-F absorption spectra using a model of optical properties of H-aggregates developed by Spano and co-workers in Refs. 28 and 30, which has been previously utilized in analysis of optical absorption and PL spectra of π-stacks which characterize crystalline regions of poly(3-hexylthiophene) (P3HT) thin films.[36,38-40] Details of the analysis of ADT-TES-F optical absorption spectra in Fig.2(a), which assumes that the only absorptive species in ADT-TES-F films are H-aggregates,[8] can be found in the Supporting Information.[20] The analysis yielded the exciton bandwidth of the absorptive H-aggregates, W_{abs}, in the ADT-TES-F films at several temperatures. The exciton bandwidth W is a measure of trap energy distribution, and it characterizes conjugation length, crystallinity, and the degree of disorder in films.[38,40,41] In particular, W should decrease as the order increases and as the trap energy distribution narrows.[28,39,40] From the exciton bandwidth W, one can calculate the strength of the resonant intermolecular coupling J in the π-π stacking direction (e.g. $J = W/4$ in the limit of weak excitonic (strong exciton-phonon) coupling, given a large number of molecules in the aggregate).[28] The bandwidth W can be

temperature-dependent due to several factors;[36] for example, in P3dHT films W decreased from 0.22 eV to 0.14 eV as the temperature decreased from 120°C to 30°C,[36] due to temperature-induced changes in the spatial correlation length l_0.[30,41] From the data in Fig.2(a), we obtained $W_{abs} \approx 0.06$ eV at 298 K, 0.05 eV at 225 K, and 0.013 eV at 100 K.[20] The values of W_{abs} obtained in ADT-TES-F films at temperatures of $\geq$225 K are on the lower (more ordered) side of the range of 0.03-0.12 eV calculated from room temperature absorption spectra in P3HT films spin coated from various solvents,[38] whereas a value of 0.013 eV at 100 K indicates a higher molecular order in the absorptive H-aggregates in ADT-TES-F films as compared to those in P3HT films at temperatures as low as 10 K.[30] As in Ref.42, we assume that the Huang-Rhys parameter S does not significantly change upon aggregation (i.e $S \approx 0.6$) in the weak excitonic coupling regime, which in our case is satisfied at all temperatures ($W_{abs} < S\omega_{eff} \approx 0.1$ eV).[29,42] In this regime, the red-shift of the aggregate spectrum from that of the isolated molecules due to nonresonant interactions is larger than the small excitonic blue-shift, resulting in an overall red-shift, as indeed observed at all temperatures (D in Fig.2(a)).[29] Therefore, the temperature dependence of W_{abs} accounts only for a small part of the temperature dependence of the A_1 and A_2 peak positions in Fig.2(b).[30] Assuming that the number of molecules in the aggregate does not change with the temperature[36] and that the thermal contraction does not significantly affect resonant interactions,[30] a considerable decrease in W_{abs} indicates a reduction in the intra-aggregate disorder at low temperatures, a finding similar to that in P3dHT.[36] The overall change in W_{abs} with the temperature was more pronounced than that of σ_{abs}. This may suggest that in the absorptive H-aggregates, the dynamic disorder due to electron coupling to low-frequency vibrational modes [43-48]

strongly contributes to W_{abs}, in contrast to σ_{abs} in the studied temperature range. Such interactions would be diminished at low temperatures reducing dynamic disorder and leading to increased spatial correlation lengths l_0 and decreased values of W_{abs}.

2. Photoluminescence: temperature dependence

PL spectra measured in an ADT-TES-F film at various temperatures are presented in Fig.3(a). There are three clearly identifiable PL bands: band 1 (~565-605 nm), band 2 (~615-655 nm), and band 3 (~680-720 nm) (labeled 1-3 in Fig.3(a)). As the temperature decreased, three main effects were observed in the PL spectra: (i) a spectral red-shift and narrowing of the spectral bands (Fig.2(b)), (ii) a significant increase in the overall PL quantum yield (QY) (Fig.3(a)), and (iii) redistribution of the relative contribution of bands 1 and 2 into the overall PL spectra (inset of Fig.3(a)). The simplest model that accounts for these observations is based on the assumption that similar to the absorptive species, the emissive species in ADT-TES-F films are disordered H-aggregates.[30] The PL spectra were analyzed similarly to the absorption spectra, by fitting with multiple Gaussians, to identify peak positions, widths, and intensities of the PL bands. Figure 2(b) shows peak positions of the PL bands 1 and 2 as a function of temperature, along with the linear fits, which yielded slopes of $(2.5\pm0.2)\times10^{-4}$ eV/K and $(3.3\pm2.6)\times10^{-5}$ eV/K and intercepts of 2.051±0.005 eV and 1.952±0.006 eV, respectively. Based on the peak positions, we assign PL bands 1-3 to emissions from a vibronically relaxed excited state S_1 to the ground state (0-0 for band 1) and to the vibronically excited levels of the electronic ground state (0-1 and 0-2 for bands 2 and 3, respectively). Given that the peak shifts of the A_1 absorption band and of the PL band 1 with the temperature occurred with

comparable rates, the Stokes shift (~0.13 eV at 100 K), defined as the energy difference between the peaks of the absorption band A_1 and of the PL band 1, was weakly temperature dependent, decreasing by less than 0.015 eV as the temperature increased from 100 K to 350 K. A major part of the observed Stokes shift in ADT-TES-F films must be related to ADT-TES-F intermolecular interactions in the solid state, as the Stokes shift in isolated ADT-TES-F molecules is considerably smaller (~0.035 eV), reflecting a relatively rigid ADT molecular core.[5] In molecular aggregates, the Stokes shift depends on the number of molecules in the aggregate, exciton bandwidth, and the amount of disorder.[30] If we assumed that the emitting species in the ADT-TES-F films are the same as the absorptive species characterized above, then Stokes shifts, due to excitonic interactions only, would be expected to yield values of $W_{abs}\exp(-S)$ = 0.008-0.033 eV at 100-298 K. These are considerably smaller than our experimental Stokes shift values of ~0.12-0.13 eV. Therefore, in ADT-TES-F films, energy migration into lower-energy trap states plays a major role in the observed Stokes shifts at all temperatures; the presence of such traps in the solid state leads to exciton localization and its subsequent transport via incoherent hopping, similar to that in amorphous materials. In amorphous organic solids, temperature-dependent Stokes shifts can be estimated from the Gaussian width σ_{abs} as $\sigma_{abs}^2/(k_BT)$ at higher temperatures (at which $\sigma_{abs}/(k_BT)<2$), followed by saturation between $(2\text{-}3)\sigma_{abs}$, depending on the exact distribution of density of states (e.g. $2.65\sigma_{abs}$ in PPV films), at lower temperatures.[49,50] This seems to describe our observations well, as the Stokes shift was about $\sigma_{abs}^2/(k_BT)$ at T >225 K and approached $2.85\sigma_{abs}$ at low temperatures, Fig.2(b). The PL 0-1 peak position had a considerably weaker temperature dependence as compared to that of the 0-0 peak position, which could be due to excitonic

effects.[29] The Gaussian width σ_{PL} of all PL bands reduced as the temperature decreased: for example, σ_{PL} of the 0-0 line reduced from ~480 cm^{-1} (0.06 eV) at 312 K to ~215 cm^{-1} (0.026 eV) at 100 K, Fig.2(b), exhibiting a considerably stronger temperature dependence than σ_{abs}.

An increase in the PL QY (Φ_{PL}) as the temperature decreased has been observed in various organic thin films; a common mechanism behind this observation is an inhibited exciton diffusion to dark states,[51] a consequence of which is a reduced nonradiative recombination at low temperatures.[34] In this case, the temperature dependence of the QY is due to a thermally activated nonradiative recombination rate k_{nr}, which can be expressed as[52]

$$k_{nr}(T)= k_{nr}^{0} + k_{nr}^{*} \exp(-\Delta_{PL}/(k_B T)), \quad (1)$$

where Δ_{PL} is the activation energy and k_{nr}^{0} and k_{nr}^{*} are constants. Then, the temperature dependence of the QY is

$$\Phi_{PL}(T) \sim k_r/(k_r + k_{nr}(T)), \quad (2)$$

where k_r is the temperature-independent radiative rate. Temperature-dependent nonradiative recombination has been previously noted in various ADT films,[5] and it is certainly relevant for the ADT-TES-F films considered here. However, if this were the only contributing process, the intensity of all three PL bands 1-3 would be expected to increase in a similar fashion as the temperature decreased.[28,30] This is not the case for our ADT-TES-F films (Fig.3). Figure 3(b) shows the temperature dependence of spectrally integrated intensities of PL bands 1-3 ($I_{0\text{-}n}$, where n = 0, 1, and 2).[30] While $I_{0\text{-}1}$ and $I_{0\text{-}2}$ had

comparable temperature dependencies, that of $I_{0\text{-}0}$ was considerably weaker. In ideal H-aggregates (no disorder), the emission from the bottom of the exciton band to the ground state (i.e. 0-0 transition) is strictly forbidden due to symmetry reasons; the 0-0 emission is allowed only if it originates at the top of the exciton band, which holds most of the oscillator strength of the transition.[28,37] In contrast, emission from 0-1 and 0-2 transitions is not restricted and is allowed from any state within the exciton band.[37] At T =0 K, after a picosecond time-scale relaxation of the exciton to low-energy states,[53] the top of the exciton band is thermally inaccessible, and the highest energy emission occurs to the first vibronic level of the ground state (i.e. 0-1 transition).[30] At T > 0 K, some 0-0 emission may occur due to thermal activation of the exciton to the top of the band. In the presence of disorder, the oscillator strength is more evenly distributed within the exciton band,[37] and 0-0 emission can be significant even at low temperatures.[30] The strength of the 0-0 emission serves as a probe of disorder and coherence of the emitting exciton. In contrast, emission from vibronic progressions, 0-1 and 0-2, is mostly of incoherent origin and is considerably less sensitive to the presence of disorder.[28,30]In disordered H-aggregates with temperature-dependent nonradiative recombination, one would expect similar temperature dependencies of $I_{0\text{-}1}$ and $I_{0\text{-}2}$ (due to that of the nonradiative recombination rate $k_{nr}(T)$ of Eq.(1)), which differ from that of $I_{0\text{-}0}$. This is indeed observed in Fig.3(b). By fitting the temperature dependence of $I_{0\text{-}1}$ with Eq.(2) (inset of Fig.3(b), left axis), we obtained an activation energy Δ_{PL} of 0.069±0.003 eV for the nonradiative recombination at temperatures ≥150 K. The temperature dependence of $I_{0\text{-}0}$ reflects a competition between thermally activated nonradiative recombination and thermally activated populating of excitonic states near the top of the band (which reduces and enhances the

emission, respectively, as the temperature increases). The inset of Fig.3(b) (right axis) shows the $I_{0\text{-}0}/I_{0\text{-}1}$ ratio as a function of temperature, fit with an exponential function ~exp(-Δ/kT), in which Δ = 0.063±0.003 eV. Similarity between Δ and Δ_{PL} suggests that populating the emissive states at the top of the exciton band and nonradiative recombination rely on the same process, such as exciton diffusion to higher-lying emissive and dark states, respectively. Relating the parameter Δ, which is a measure of disorder in emissive H-aggregates, to their exciton bandwidth W_{em} via $\Delta = W_{em}\exp(-S)$ yields W_{em} = 0.115 eV. A larger exciton bandwidth of the emissive species, W_{em}, as compared to that of the absorptive species, W_{abs}, suggests that the emissive aggregates are more disordered than the absorptive ones. Similar findings have been reported in P3HT films (W_{abs} = 0.12 eV and W_{em} = 0.28 eV).[30] The value of W_{em} in ADT-TES-F films, which is considerably smaller than that in P3HT films, is consistent with a stronger temperature dependence of the $I_{0\text{-}0}/I_{0\text{-}1}$ ratio in ADT-TES-F films as compared to P3HT films. From the $I_{0\text{-}0}/I_{0\text{-}1}$ ratios at low temperatures, we calculated the spatial correlation parameter β and the correlation length l_0 ($l_0 = -1/\ln\beta$, given in the dimensionless units of lattice spacing)[41] using methodology developed in Refs.28 and 30 (see Supporting Information for details).[20] In the disordered H-aggregates model, the parameter β ranges from 0 when l_0 = 0 (no spatial correlation between molecules; high intra-aggregate disorder) to 1 when $l_0 = \infty$ (infinite spatial correlation; no intra-aggregate, thus only inter-aggregate disorder). In our ADT-TES-F films, values of $\beta \approx 0.75\text{-}0.77$ and of $l_0 \approx 3.8\text{-}5.0$ were obtained which indicate spatial correlations over ~4-5 molecules.[30]

To gain insight into the relevant time-scales for temperature dependence of the PL emission, we measured PL lifetimes of the emissive aggregates in several PL spectral

regions (selected by filters, Sec. II.B) at various temperatures. In molecular aggregates, the PL decay is multiexponential due to fluctuations in the radiative decay rates of different excitonic states within the exciton bandwidth and to an interplay between radiative rates and intraband relaxation rates.[54,55] In ADT-TES-F films, the PL decays could be fit with a bi-exponential function ($a_1 \exp(-t/\tau_1)+a_2 \exp(-t/\tau_2)$) in all PL spectral regions and at all temperatures.[5,8,9,56] Slightly faster decays (shorter τ_1 and τ_2) were observed from the PL band 1 than from the rest of the PL spectrum at all temperatures (Fig.4(a)), due to a residual exciton relaxation towards lower energies.[37] Figure 4 shows the temperature dependence of the PL lifetimes, τ_1 and τ_2 (a), and their amplitudes, a_1 and a_2 (b), obtained from lifetime decays of the entire PL spectrum; the average lifetime τ_{av} calculated as $\tau_{av} = (a_1\tau_1 + a_2\tau_2)/(a_1+a_2)$ is also included in the figure. At all temperatures, both τ_1 and τ_2 values were lower than the radiative lifetime of 13.4 ns for isolated ADT-TES-F molecules (dash-dotted line in Fig.4(a)). Both lifetimes increased by a factor of ~1.5-1.7 as the temperature decreased from 300 K to 100 K, which suggests that they were affected by a similar thermally-activated nonradiative recombination process. At low temperatures, the longer time constant τ_2 approached a range of ~9-12 ns, similar to those obtained from single-exponential fits to PL decays of isolated ADT-TES-F molecules in solutions and in PMMA films,[5,8]whereas the shorter time constant τ_1 was still considerably below these values. Weak temperature dependence of the PL lifetimes, as opposed to that of the PL QY in Fig.3(a), suggests that only a small portion of nonradiative recombination occurred at nanosecond time scales. In contrast to lifetimes, the amplitudes a_1 and a_2 exhibited different temperature dependencies: a_1 significantly increased as the temperature decreased from 300 K to 100 K, while a_2 was affected

minimally. The observed changes in a_1 indicate that most nonradiative recombination responsible for strong temperature dependence of the PL QY occurred at shorter time scales than the time resolution of our PL lifetime measurements (~200 ps).[57,58] Based on the observations above, the PL lifetimes τ_1 and τ_2 may be tentatively assigned to excitons that sample the entire thermally accessible portion of the exciton bandwidth and only the top part of it, respectively (Sec. IV.A, Fig.11). At higher temperatures the bottom population of the exciton band (related to a_1) is depleted due to thermally activated diffusion to dark states. At low temperatures, the nonradiative recombination is mostly deactivated, leading to larger values of a_1. The population of the emissive states at the top of the exciton band (related to a_2) relies on thermal excitation of the population at the bottom of the band. At higher temperatures, the probability of this thermal excitation is higher, but the nonradiative recombination is also stronger. Thus, the temperature dependence of a_2 is determined by the balance of these two processes.

3. Photoluminescence: electric field dependence

In order to investigate the propensity of the emissive exciton to dissociate, we measured PL spectra and lifetimes under applied electric field. Figure 5 shows the PL spectra obtained at various applied electric fields at 190 K. A PL quenching of up to ~50% at an electric field of 1.8×10^5 V/cm was observed. At either temperature no changes were seen in absorption spectra at the same electric fields, which rules out the Stark effect.[57] From the integrated PL spectra measured in the presence and in the absence of electric field ($I_{PL}(E)$ and $I_{PL}(0)$, respectively), we calculated the parameter Q, which quantifies the amount of the PL quenching, using[57,59-61]

$Q = 1\text{-}I_{PL}(E)/I_{PL}(0)$ (3).

The inset of Fig.5 shows the electric field dependence of Q at several temperatures. No significant temperature dependence of Q was observed in the ~100-200 K temperature region. Interestingly, at above ~210 K, the electric field-induced PL quenching was dramatically reduced, and no quenching was observed at >225 K in the same electric field range (inset of Fig.5).[5] The electric field dependence of Q can help identify the nature of the exciton; for example, linear (quadratic) electric field dependence of Q has been reported in charge-transfer (neutral) excitons dissociating into free carriers.[57,58] The dependence of Q on the electric field observed in ADT-TES-F films at low temperatures and at electric fields of above $\sim 10^5$ V/cm is considerably stronger than quadratic and can be better described by a one-dimensional model for tunneling through a parabolic potential barrier:[62,63]

$$Q = (1+a \exp(\pi\sqrt{m^*}E_b^{3/2}/(2\sqrt{2}\hbar eE)))^{-1} \quad (4),$$

where a is a constant (free fit parameter), m* is the effective mass, ħ is the Planck constant, e is the unit charge, and E_b is the exciton binding energy. The fit of the 100 K data with Eq.(4), which yielded $E_b = 0.097 \pm 0.009$ eV (assuming $m^* = m_e$, where m_e is the electron mass), is shown in the inset of Fig.5. Similar fits to data from various ADT-TES-F films at temperatures between 100 K and 200 K yielded binding energies E_b in the range of 0.07-0.1 eV, which were sample-dependent, rather than temperature-dependent. In the range of electric fields studied, the data could not be fit with Eq.(4) at temperatures above ~210 K. In addition, no changes in the PL lifetimes were observed as a function of applied electric field at either temperature, and the electric field-induced changes in the

PL emission were mostly incorporated in those of the amplitude a_1, thus occurring within ~200 ps, limited by the time resolution of our PL lifetime measurements.[58] As there was no indication of an increase in the free carrier yield accompanying the PL quenching (discussed below),[60] we attribute the fast PL quenching to electric field-enhanced nonradiative recombination, as previously observed in conjugated polymers,[64] which favorably competes with the thermally-activated nonradiative recombination at low temperatures (Sec. IV.A, Fig.11).

4. Transient photocurrent

Figure 6(a) shows the transient photocurrents in an ADT-TES-F film at various temperatures, obtained under 355 nm 500 ps pulsed illumination at an electric field of 1.2×10^5 V/cm. The rise time was limited by the laser pulse width, at all temperatures, which suggests sub-500 ps charge carrier photogeneration, consistent with our previous findings.[5-7,22] Three main changes in the transient photocurrent were observed as the temperature decreased: (i) the peak amplitude decreased (Fig.6(a)), (ii) the initial decay dynamics became faster and more pronounced (inset of Fig.6(a)), and (iii) the electric field dependence of the peak amplitude became stronger (Fig.6(b)). The peak photocurrent $I_{ph,peak}$ can be expressed as[49]

$$I_{ph,peak} = N_{abs} e\mu\eta E/L, \quad (5)$$

where N_{abs} is the number of absorbed photons during the pulse, e is the electric charge, μ is the sum of electron and hole mobilities (here dominated by the hole mobility)[3-5,11,18,22] averaged over the pulse duration, E is the electric field, and L is the gap between the electrodes. The parameter η is the photogeneration efficiency, which includes carrier loss

due to trapping and recombination during the pulse duration.[6,27,65] The product of the mobility and charge photogeneration efficiency, μη, calculated from the data in Fig.6(a) using Eq.(5), yielded ~0.002 $cm^2/(Vs)$ at an electric field of 1.2×10^5 V/cm at 298 K. At 98 K, and at the same electric field, it was a factor of ~7-8 lower. The observed μη values were about an order of magnitude lower than those measured with sub-30 ps time resolution in drop-cast polycrystalline ADT-TES-F films at 100 fs photoexcitation.[5] This is due to a stronger carrier loss over a 500 ps pulse duration and lower charge carrier mobilities in spin-coated films studied here. For example, the effective hole mobility values extracted from space-charge-limited currents (SCLC)[5,22] in spin-coated ADT-TES-F films at room temperature were in the range of 0.01-0.02 $cm^2/(Vs)$ (as compared to 0.033-0.092 $cm^2/(Vs)$ in drop-cast films).[5] These values are consistent with saturation mobility values obtained from TFT characteristics of similarly prepared spin-coated ADT-TES-F films on untreated Au electrodes.[4,11,12] In the transient photocurrent measurements, which probe charge carrier dynamics shortly after pulsed photoexcitation, i.e. before the carriers fully relax and equilibrate, the SCLC effective mobility values should be considered as a lower limit of mobility μ in the μη-product calculated from the peak of the transient photocurrent. Thus, if μ_{min} is ~0.02 $cm^2/(Vs)$, then the room-temperature photogeneration efficiency η is below ~0.1, consistent with values observed in similar experiments with other organic crystals and films.[5,66,67]

The electric field dependence of the peak photocurrent $I_{ph,peak}$ could be due to that of the mobility μ, the photogeneration efficiency η, or both. Figure 6(b) shows the electric field (*E*) dependence of μη calculated from $I_{ph,peak}$ using Eq.(5) at several temperatures. At 298 K, the electric field dependence of μη was weak, consistent with results of similar

experiments performed with various ADT films,[22] tetracene crystals,[66] and conjugated polymers.[68,69] As the temperature decreased, the electric field dependence of $\mu\eta$ became more pronounced. Although in our experiments μ and η cannot be separated, the data are more consistent with the assignment of electric field dependence of $\mu\eta$ to that of the mobility μ.[70] For example, at all temperatures, the electric field dependence of $\mu\eta$ could be fit well with the Poole-Frenkel function, which describes field-dependent mobility $\mu \sim \exp(\gamma\sqrt{E})$ in disordered materials (Fig.6(b)).[21,71,72] The parameter γ is given by

$$\gamma = B(1/(k_BT) - 1/(k_BT_0)) \quad (6),$$

where T_0 and B are constants. Inset of Fig.6(b) shows the temperature dependence of the parameter γ, obtained from the fits of the data in Fig.6(b) with the Poole-Frenkel function. The $\gamma(T)$ dependence was fit with Eq.(6), yielding $T_0 = 600$ K and $B = 1.35\times10^{-4}$ eV(cm/V)$^{1/2}$, similar to those in conjugated polymers.[71]

Figure 7 shows the temperature dependence of the peak photocurrent $I_{ph,peak}$ normalized by that at 300 K, measured in pristine ADT-TES-F films and ADT-TES-F-based composites. At an electric field of 1.2×10^5 V/cm, the photocurrent activation energy Δ_{ph} obtained from fitting of the peak photocurrent in a pristine ADT-TES-F film with the Arrhenius-type function, $I_{ph,peak} \sim \exp(-\Delta_{ph}/(k_BT))$, yielded $\Delta_{ph} = 0.025\pm0.002$ eV (inset of Fig.7). It should be noted that the activation energy Δ_{ph} could be due to the temperature dependence of the carrier mobility μ, photogeneration efficiency η, or both. From Fig.7, the two composites under study (ADT-TES-F/C_{60} and ADT-TES-F/ADT-TIPS-CN, Sec. III.B and III.C) exhibited temperature dependencies of the peak photocurrent similar to that of the pristine ADT-TES-F films, in spite of differences in charge carrier

photogeneration mechanisms in these composites (discussed below). This suggests that the activation energy Δ_{ph} is mostly due to a thermally activated mobility, rather than the photogeneration efficiency, which would be consistent with the Poole-Frenkel electric field dependence of mobility established above[21] and with observations of thermally activated mobility in ADT-TES-F TFTs.[11] As such, Δ_{ph} provides a measure of the energy distribution of charge traps participating in the hopping transport. The activation energy Δ_{ph} increased as the electric field decreased due to electric field-assisted detrapping, which has been observed in a variety of organic films.[72,73]

The decay dynamics of the transient photocurrent is due to charge carrier trapping and recombination.[49] Similar to other functionalized ADT and pentacene derivatives,[6,7,22,27,74] ADT-TES-F films exhibited a fast initial decay followed by a slow component, which persisted to at least microsecond time scales and was characterized by a power law function ($\sim t^{-b}$) at all temperatures. As the temperature decreased, the fast decay component became more pronounced due to charge carriers being frozen in traps, thus ceasing to contribute to the photocurrent at nanosecond time scales. The power-law decay has been previously observed in various organic crystals and films[27,74-76] and attributed to dispersive transport. The power-law exponent *b* extracted from the slower decay component of the photocurrent[5,7,22] was only weakly temperature dependent, increasing from ~0.2 at 298 K to ~0.3 at 98 K. Similar behavior has been previously observed in functionalized pentacene crystals,[74] C_{60} thin films,[77] and conductive polymers.[78] Such behavior is inconsistent with the multiple trapping model, in which $b = 1-\alpha$, where $\alpha = k_BT/E_t$ with E_t being a measure of the exponential distribution of trap state energies.

Instead, it suggests that at above ~5 ns after excitation the charge carriers move via non-activated tunneling along sites with similar energies.[79]

B. ADT-TES-F/C_{60} films

In this section, we explore the effects of photoinduced charge transfer from ADT-TES-F to C_{60} on exciton dynamics, charge carrier photogeneration efficiency, and time-resolved charge carrier dynamics in composite films.

1. Optical and photoluminescent properties

Optical absorption spectra of the ADT-TES-F/C_{60} (2%) films were similar to those of pristine ADT-TES-F films in Fig.2(a), indicative of no significant interaction between the ADT-TES-F and C_{60} molecules in the ground state. The PL QY was about a factor of ~10 lower than that in pristine ADT-TES-F films under the same conditions. The PL quenching in fullerene-containing composites has been reported in various conjugated polymer/fullerene blends and attributed to ultrafast photoinduced electron transfer from the donor (polymer) to the acceptor (fullerene) molecules.[80-82] A similar photoinduced electron transfer process occurred in ADT-TES-F/C_{60} composites,[7] with C_{60} acting as a strong acceptor in these films (Fig.1(b)). The spectrum of the residual PL emission in ADT-TES-F/C_{60} composites (which has not been quenched via photoinduced electron transfer) and its temperature dependence were identical to those of the pristine ADT-TES-F films in Fig.3, confirming sole contribution of ADT-TES-F to the PL properties of ADT-TES-F/C_{60} films.

2. Transient photocurrent

The transient photocurrents in an ADT-TES-F/C_{60} film at various temperatures, obtained under 355 nm 500 ps pulsed illumination at an electric field of 1.2×10^5 V/cm, are shown in Fig.8. The peak photocurrent was a factor of ~2-3 higher than that in pristine ADT-TES-F films under similar conditions, due to improved charge carrier photogeneration.[7] Faster initial decay (limited by the pulse width) as compared to that in pristine ADT-TES-F films was observed, consistent with previous studies,[7] which has been attributed to enhanced initial carrier trapping and recombination in this composite. The trends in the temperature dependence of the photocurrent were similar to those in pristine ADT-TES-F films: as the temperature decreased, the peak photocurrent decreased (with the activation energy Δ_{ph} similar to that in pristine ADT-TES-F films, Fig.7), and the contribution of the fast initial decay into the transient became more pronounced, whereas the slower power-law decay component[7] was weakly temperature dependent. Thus, physical mechanisms that determine the temperature dependence of the transient photocurrent in ADT-TES-F/C_{60} composites are similar to those in pristine ADT-TES-F films.

C. ADT-TES-F/ADT-TIPS-CN films

In this section, we explore the effects of exciplex formation that occurs as a result of a photoinduced partial charge transfer between ADT-TES-F and ADT-TIPS-CN, on time-resolved exciton dynamics, charge carrier photogeneration, and charge transport in composite films.

1. Optical and photoluminescent properties

Optical absorption spectra of ADT-TES-F/ADT-TIPS-CN (2%) films were similar to those of the pristine ADT-TES-F films in Fig.2(a), and no significant ground-state charge transfer was observed.[7] The PL spectra obtained at various temperatures are presented in Fig.9(a). It has been previously shown that the PL emission in this composite is strongly dominated by emission from an exciplex formed between the HOMO of the ADT-TES-F (donor) and LUMO of the ADT-TIPS-CN (acceptor) molecules.[9] As the temperature decreased, the PL spectra red-shifted with a rate of $(2.5\pm0.1)\times10^{-4}$ eV/K, similar to that in the pristine ADT-TES-F films (Sec. III.A.2), and the overall PL QY increased. Assuming that the temperature dependence of the PL QY is mostly due to that of the nonradiative recombination rate (Eq.(1)), we fit the integrated PL spectra (left inset of Fig.9(a)) with Eq.(2), which yielded the activation energy $\Delta_{PL} = 0.08\pm0.02$ eV, comparable to ~0.07 eV in pristine ADT-TES-F films (inset of Fig.3(b)). Most change in the exciplex emission in ADT-TES-F/ADT-TIPS-CN composites occurred at temperatures above ~250 K, followed by QY saturation at lower temperatures.

Our previous PL studies showed that the exciplex emission in ADT-TES-F/ADT-TIPS-CN films is characterized by a lifetime τ_{exci} of ~19-22 ns at room temperature.[9] Figures 9(b) and (c) show PL lifetimes τ_1 and τ_2 and the corresponding amplitudes a_1 and a_2,obtained from bi-exponential fits of the PL decay dynamics over the entire PL emission spectrum of an ADT-TES-F/ADT-TIPS-CN film, as functions of temperature. The values and behavior of the short time constant τ_1 are consistent with those of the average time τ_{av} in pristine ADT-TES-F films (Fig.4(a)) and are due to the residual

contribution of the PL emission from ADT-TES-F aggregates. This assignment is confirmed by our observation of ADT-TES-F aggregate-like PL decays in the 550-610 nm part of the PL emission of the ADT-TES-F/ADT-TIPS-CN films. The contribution of ADT-TES-F aggregates, as revealed by the PL decay dynamics measured at various emission wavelengths selected by filters (Sec. II.B), persisted to at least ~700 nm. At >700 nm, the PL decays were solely due to the exciplex (τ_{exci}) and were single-exponential such that the lifetimes $\tau_{exci} = \tau_2$. As the temperature decreased from 300 K to 100 K, the exciplex lifetime τ_{exci} increased by a factor of ~1.3 and the amplitude a_2 increased by a factor of ~2, which suggests that a considerable part of the temperature dependence of the PL emission is due to processes occurring on sub-200 ps time scales, not accessible in our PL lifetime measurements. The similarity between temperature dependencies of the amplitudes a_1 (due to emissive ADT-TES-F aggregates) and a_2 (due to the ADT-TES-F/ADT-TIPS-CN exciplex) may indicate that these are related to the same process. For example, if a relaxed ADT-TES-F exciton is a precursor to the exciplex, then the behavior of both a_1 and a_2 would be affected by thermally-activated nonradiative recombination of the ADT-TES-F exciton due to exciton diffusion to dark states (Sec. III.A.2 and IV.A).

To establish effects of the electric field on the exciplex, we measured PL spectra and lifetimes under various applied electric field strengths and at various temperatures. The parameter Q (Eq.(3)), which characterizes the degree of electric field-induced PL quenching, reached ~0.06-0.07 at the highest applied field of 1.6×10^5 V/cm, at all temperatures studied (right inset of Fig.9(a)). Similar to pristine ADT-TES-F films, the dependence of Q on the electric field in the ADT-TES-F/ADT-TIPS-CN composite was

stronger than quadratic at fields above ~ 5×10^4 V/cm, and the fit of the data to Eq.(4) (assuming $m^* = m_e$) yielded a binding energy of $E_b = 0.045\pm0.005$ eV at 98 K, which did not appreciably change with temperature. Interestingly, the PL lifetime measurements revealed that at 98 K, the exciplex lifetime did not change with the electric field, and all electric field-induced changes were incorporated in the amplitude a_2, thus occurring at sub-200 ps time scales not resolved by our experiments. This could be due to electric field-induced nonradiative recombination of the relaxed ADT-TES-F exciton (the exciplex precursor), an effect similar to that in pristine ADT-TES-F films at low temperatures. At room temperature, a small change in the exciplex lifetime τ_{exci} (from ~20 ns at zero electric field to ~18 ns at 1.6×10^5 V/cm) was observed, indicative of exciplex dissociation. This dissociation creates a slow charge carrier generation channel, which persists during the exciplex lifetime (Fig.10, Sec. III.C.2) in ADT-TES-F/ADT-TIPS-CN films, not existent in pristine ADT-TES-F films.[7,9]

2. Transient photocurrent

Figure 10 shows the transient photocurrents in an ADT-TES-F/ADT-TIPS-CN (2%) film at various temperatures, obtained under 355 nm 500 ps illumination at an electric field of 1.2×10^5 V/cm. At room temperature, the photocurrent at ~1 ns after photoexcitation was about a factor of ~2 lower than that in pristine ADT-TES-F films, and the peak photocurrent was reached at ~20 ns after the photoexcitation, due to the emergence of a slower component in the photocurrent rise dynamics. This component has been previously attributed to slow charge carrier photogeneration due to exciplex dissociation over the period of exciplex lifetime (~20 ns), which contributed about ~5% of the photocurrent amplitude under these conditions.[9] At times above ~20 ns, a slow power-

law decay was observed, with a power-law exponent b <0.03. Drastic slowing down of the photocurrent decay dynamics in the ADT-TES-F/ADT-TIPS-CN composite as compared to that in pristine ADT-TES-F films has been attributed to inhibited charge carrier recombination in the composite.[7] The trends in the temperature dependence of the photocurrent were similar to those in the pristine ADT-TES-F films, indicative of similar charge transport properties. In particular, as the temperature decreased, the photocurrent at ~1 ns after photoexcitation decreased with the activation energy Δ_{ph} similar to that in pristine ADT-TES-F films (Fig.7), and the initial decay dynamics (at <5 ns) became faster. At low temperatures, the contribution of charge carriers produced via exciplex dissociation to the photocurrent was no longer observed, due to less efficient exciplex dissociation and more pronounced carrier loss in deep traps.

IV. DISCUSSION

In this section, we will combine observations of Sec. III into a physical picture of temperature-dependent photoexcited charge carrier and exciton dynamics in pristine ADT-TES-F films and ADT-TES-F-based guest-host composite films.

A. Charge carrier and exciton dynamics

The observed PL and nanosecond time-scale photoconductive properties of pristine ADT-TES-F films and ADT-TES-F-based composites are consistent with the following picture (Fig.11). The initial photoexcitation of ADT-TES-F was distributed among the excitonic channel (responsible for PL), fast photoconductive channel (responsible for fast photocurrents), and other possible channels (such as photoinduced electron transfer in

ADT-TES-F/C_{60} films). This distribution of the photoexcitation occurred on the picosecond or sub-picosecond time scales.

1. Charge carrier dynamics

Upon photoexcitation of a higher excited state of ADT-TES-F (Fig.11), the charge carriers were created on sub-500 ps (most likely on sub-30 ps or faster)[6,7,27,65,83] time-scales, with a photogeneration efficiency $\eta<0.1$, which is independent of temperature and electric field. In order to distinguish between direct charge carrier photogeneration[84] and ultrafast hot exciton dissociation,[85] both of which would be consistent with these observations, measurements of the wavelength dependence of time-resolved photocurrent would be necessary, which is beyond the scope of this article. Note, however, that previous studies revealed wavelength-independent photogeneration at sub-ps time scales in single crystals and films of pentacene and functionalized pentacene derivatives, which is more consistent with direct photogeneration.[65] The photogeneration efficiency was enhanced in the presence of C_{60} due to fast photoinduced electron transfer (k_{ET}) from ADT-TES-F to C_{60} (e.g. by a factor of 2-3 in the ADT-TES-F/C_{60} (2%) composite). In the ADT-TES-F/ADT-TIPS-CN composite, after exciplex formation (k_{exci}), a small additional contribution (η_{exci}) to charge carrier photogeneration due to exciplex dissociation at time scales of <20 ns was observed at room temperature, but not at low temperatures. In all three materials studied, electric field-induced dissociation of emissive excitons investigated by our PL measurements did not play an important role in fast charge carrier generation.

In all materials, at time scales of ~0.5-5 ns, the charge carrier transport proceeded by hopping via shallow traps characterized by weakly thermally-activated (Δ_{ph}~0.025 eV) and electric field-dependent charge carrier mobility. At time scales above ~5 ns after photoexcitation, the charge propagated within a narrow energy manifold by non-activated tunneling.[50] At low temperatures, a significant number of charge carriers were frozen in traps and did not contribute to charge transport at nanosecond time scales.

2. Exciton dynamics

In pristine ADT-TES-F films, both the absorptive and the emissive species were identified to be disordered H-aggregates formed by π-stacked ADT-TES-F molecules in the crystallites, with the emissive aggregates being more disordered than the absorptive. Fast nonradiative recombination, due to thermally-activated exciton diffusion (e.g. intra-aggregate) to dark states on sub-200 ps time scales (limited by the time resolution of our setup), was observed at higher temperatures. Slow nonradiative recombination, due to weakly thermally-activated transitions (e.g. inter-aggregate) to dark states on the nanosecond time scales, was also observed (Fig.11). At low temperatures, it was possible to reactivate the fast nonradiative recombination process by applying an electric field, which induced PL quenching. At high temperatures, fast thermally activated nonradiative recombination overpowered electric field-activated recombination, and no electric field-induced PL quenching was observed. In ADT-TES-F/C_{60} composites, emissive species were the same as those in pristine ADT-TES-F films, and all considerations above applied. However, the overall PL was strongly quenched due to efficient photoinduced electron transfer (k_{ET}) from ADT-TES-F to C_{60}. In ADT-TES-F/ADT-TIPS-CN composites, the PL emission at all temperatures was dominated by that of an exciplex

formed between the HOMO of ADT-TES-F and LUMO of ADT-TIPS-CN. The relaxed ADT-TES-F exciton appears to be a precursor state for the exciplex, as schematically shown in Fig.11, leading to similar features in the temperature and electric field dependence of the PL of the exciplex and of ADT-TES-F aggregates.

B. Role of disorder in exciton and charge carrier dynamics

In pristine ADT-TES-F films, both absorptive and emissive H-aggregates were affected by disorder. Contributions of both weakly temperature-dependent static disorder due to solid-state structural defects[47] and strongly temperature-dependent dynamic disorder due to electron coupling to low-frequency vibrational modes[43] to spectral linewidths and exciton bandwidths were observed (Sec.III.A.1 and III.A.2). In emissive π-stacks, the exciton bandwidth W_{em} was larger than that in the absorptive π-stacks (W_{abs}). Both W_{abs} and W_{em} (≤0.06 eV and 0.115 eV, respectively) in ADT-TES-F films were smaller than the corresponding values in crystalline P3HT films in Ref. 30 (W_{abs} = 0.12 eV and W_{em} = 0.28 eV). In P3HT films, the difference between W_{abs} and W_{em} was attributed to a difference in conjugation lengths of the polymeric chains that comprise the absorptive and emissive H-aggregates. In particular, it was estimated that in the emitting π-stacks the conjugated segments were about a factor of 2 smaller than the 20-30 repeat units in the π-stacks of absorptive aggregates.[30] This estimate was based on the analytical model that predicts that in dimers formed by parallel chains of length L_c separated by a distance R, at $L_c > R$ the exciton bandwidth W scales as $1/L_c$ or $1/L_c^{1.8}$, depending on the approximation,[86] and a $1/L_c$ dependence was assumed in Ref.30. In the case of very short chains ($L_c < R$), the exciton bandwidth scales linearly with the chain length. Oligomers

such as ADT-TES-F fall into an intermediate regime, depending on the number of conjugated units and R, so that the analytical relationship between W and L_c is less straightforward, but relatively weak.[86] Therefore, in ADT-TES-F films, we attribute differences in W_{abs} and W_{em} to differences in the amount of disorder in the absorptive and emissive aggregates, with the emissive aggregates being more disordered. It has been shown that relative shifts and π-plane orientations of the adjacent molecules significantly contribute to the exciton bandwidth due to changes in wave function overlap causing changes in intermolecular interactions.[87] Due to the 2D nature of the π-stacking in ADT-TES-F crystallites,[10] there is a distribution of interplanar distances and relative molecular shifts, which contributes to static disorder. Additionally, in these functionalized materials electron-phonon coupling introduces strongly temperature-dependent dynamic disorder that significantly affects intermolecular coupling[44] and thus, the exciton bandwidth as is apparent from the temperature dependence of W_{abs}, which dramatically decreases as the temperature decreases (Sec. III.A.1). In emissive ADT-TES-F aggregates, additional insight into the disorder is provided by the spatial correlation parameter β≈0.75-0.77 and spatial correlation length l_0 =3.8-5.0, which indicate exciton delocalization over 4-5 molecules (Sec.III.A.2). These values were slightly smaller than β = 0.88 and l_0 =7.8 (corresponding to delocalization over ~8 molecules) in H-aggregates formed by π-stacked molecules in the crystalline regions of P3HT films,[30] although the exciton bandwidth W_{em} in P3HT was considerably higher than that in ADT-TES-F films (0.28 eV and 0.115 eV, respectively). This suggests slightly higher intra-aggregate disorder (leading to smaller values of β and l_0), due to the 2D nature of π-stacking and the

presence of dynamic disorder, but considerably lower inter-aggregate disorder (leading to smaller exciton bandwidths *W*) in ADT-TES-F as compared to P3HT films.

In contrast to exciton dynamics, the dynamic disorder did not seem to play a crucial role in charge carrier mobility observed at nanosecond time-scales after pulsed photoexcitation, as no improvement in charge carrier mobility was observed upon a decrease in dynamic disorder at low temperatures. Instead, the charge carrier transport at nanosecond time-scales was mostly affected by the static disorder, as expected for a hopping transport of localized charge carriers.[88] The energy distribution of trap sites contributing to charge transport in ADT-TES-F films at ~1 ns after photoexcitation (~0.025 eV) was considerably narrower than that in polymers (e.g. 0.48 eV in PPV)[71] including high-quality crystalline P3HT and P3dHT films (0.05-0.12 eV).[36,89] Given that the overall charge carrier mobility in polycrystalline films is limited by the mobility in more disordered regions near grain boundaries and/or in crystallites with orientations unfavorable for in-plane charge transport such as (111) in ADT-TES-F,[21] the observed narrow trap distribution reflects a better order in these low-mobility regions in ADT-TES-F as compared to P3HT or P3dHT films. Nevertheless, the presence of such regions prevented our observation of a change in charge transport properties as a result of a subtle solid-solid phase transition occurring at 294 K, previously reported in ADT-TES-F single crystals and films composed of large crystallites with an exclusively (001) orientation.[11]

V. SUMMARY

We have presented a physical picture of exciton and charge carrier dynamics in spin-coated ADT-TES-F, ADT-TES-F/C_{60} (2%), and ADT-TES-F/ADT-TIPS-CN (2%) thin

films obtained through measurements and analysis of the temperature dependence of their optical absorption, PL, and photoconductive properties. Optical absorption and PL properties of pristine ADT-TES-F films were dominated by those of disordered H-aggregates. In absorptive aggregates, the exciton bandwidth W_{abs}, estimated from the ratio of intensities of A_1 and A_2 absorption bands (Fig.2(a)), decreased from ~0.06 eV at 300 K to 0.013 eV at 100 K due to a reduced dynamic disorder at low temperatures. Optical properties of these aggregates were also affected by weakly temperature-dependent static disorder due to solid-state defects. The emissive aggregates were more disordered than the absorptive ones, with the exciton bandwidth W_{em} of ~0.115 eV, as estimated from the ratios of PL emission from the 0-0 and 0-1 transitions (Fig.3). In these aggregates, the analysis revealed spatial correlation lengths of ~3.8-5.0, indicative of exciton delocalization over 4-5 molecules. Properties of these aggregates were also affected by the dynamic disorder. Strong temperature dependence of PL due to thermally activated nonradiative recombination was observed. The dominant mechanism of nonradiative recombination was exciton diffusion to dark states with a thermal activation energy of ~0.07 eV, which occurred at sub-200 ps time-scales (limited by the time resolution of our PL lifetime measurements). At low temperatures, electric field-induced tunneling competed favorably with thermally activated diffusion, leading to a partial PL quenching at electric fields above 10^5 V/cm (Fig.5).

In ADT-TES-F/C_{60} composites, the PL was considerably quenched due to fast photoinduced electron transfer from ADT-TES-F to C_{60}. The PL properties of the residual emission were similar to those of ADT-TES-F aggregates in pristine ADT-TES-F films. In ADT-TES-F/ADT-TIPS-CN composites, the PL emission was dominated by

that due to an exciplex formed between ADT-TES-F and ADT-TIPS-CN (Fig.9). The ADT-TES-F relaxed exciton appears to serve as a precursor to the exciplex. Thus, sub-200 ps thermally-activated nonradiative recombination with activation energies of ~0.08 eV and electric field-induced PL quenching at fields above 10^5 V/cm were observed in ADT-TES-F/ADT-TIPS-CN films, similar to those in pristine ADT-TES-F films. Weak electric field-induced PL quenching was observed during the exciplex lifetime of ~20 ns at higher temperatures due to exciplex dissociation into free carriers (Fig.10).

In all materials, the charge carriers were generated on sub-500 ps time scales (limited by the laser pulse width) (Figs.6,8,10) with the photogeneration efficiency independent of the electric field and temperature. In pristine ADT-TES-F films, the product of the charge carrier mobility and photogeneration efficiency was ~0.002 $cm^2/(Vs)$ at room temperature. Given the lower limit of charge carrier mobility of ~0.02 $cm^2/(Vs)$ in these films, the photogeneration efficiency was below ~0.1. In ADT-TES-F/C_{60} (2%) films, it was a factor of 2-3 higher. No evidence of emissive exciton dissociation contributing to fast charge carrier generation was observed. In ADT-TES-F/ADT-TIPS-CN (2%) films, the efficiency of fast charge carrier photogeneration was reduced, but an additional slow charge carrier photogeneration process developed on time scales of ~20 ns due to exciplex dissociation at room temperature. In all materials, the charge transport at 0.5-5 ns after photoexcitation was dominated by electric field- and temperature-activated hopping via shallow traps with an activation energy of ~0.025 eV at 1.2×10^5 V/cm, relaxing to iso-energetic tunneling at time scales above ~5 ns. No significant effect of a temperature-dependent dynamic disorder on charge carrier mobility was observed.

In conclusion, the main findings of the paper can be summarized as follows: 1) optical and PL properties in pristine ADT-TES-F films are due to disordered H-aggregates formed by π-stacked ADT-TES-F molecules, with both static and dynamic disorder contributing to properties of the aggregates; 2) fast sub-500 ps charge carrier photogeneration in pristine ADT-TES-F or its composites does not rely on the dissociation of ADT-TES-F emissive excitons; a small contribution of ADT-TES-F/ADT-TIPS-CN exciplex dissociation to charge carrier photogeneration was observed in ADT-TES-F/ADT-TIPS-CN composites at ~20 ns time-scales; and 3) at 0.5-5 ns after photoexcitation, charge transport is affected by static disorder and proceeds by hopping via sites with narrow energy distribution (~0.025 eV) evolving into non-activated tunneling at longer time-scales, in all materials studied.

Our measurements revealed that the dynamics of excited states at picosecond and sub-picosecond time scales has a considerable contribution into optical and electronic properties of ADT-TES-F-based films. Therefore, ultrafast spectroscopy would be needed to determine early time evolution[90,91] of excitonic and charged states and refine the physical picture of exciton and charge carrier dynamics in these materials.

ACKNOWLEDGMENTS

We thank Prof. B. Gibbons for x-ray diffraction and Dr. L. Prisbrey for atomic force microscopy measurements. This work was supported by NSF via CAREER program (Grant No. DMR-0748671), ONAMI via the Office of Naval Research (Grant No. N00014-07-1-0457), and the Office of Naval Research (Grant No.N00014-11-1-0329).

[1] H. E. Katz and J. Huang, Annual Review of Materials Research **39,** 71 (2009).

[2] A. C. Arias, J. D. MacKenzie, I. McCulloch, J. Rivnay, and A. Salleo, Chem. Rev. **110,** 3 (2010).

[3] S. K. Park, D. A. Mourey, S. Subramanian, J. E. Anthony, and T. N. Jackson, Appl. Phys. Lett. **93,** 043301 (2008).

[4] D. J. Gundlach, J. E. Royer, S. K. Park, S. Subramanian, O. D. Jurchescu, B. H. Hamadani, A. J. Moad, R. J. Kline, L. C. Teague, O. Kirillov, C. A. Richter, J. G. Kushmerick, L. J. Richter, S. R. Parkin, T. N. Jackson, and J. E. Anthony, Nat. Mater. **7,** 216 (2008).

[5] A. D. Platt, J. Day, S. Subramanian, J. E. Anthony, and O. Ostroverkhova, J. Phys. Chem. C **113,** 14006 (2009).

[6] J. Day, S. Subramanian, J. E. Anthony, Z. Lu, R. J. Twieg, and O. Ostroverkhova, J. Appl. Phys. **103,** 123715 (2008).

[7] J. Day, A. D. Platt, O. Ostroverkhova, S. Subramanian, and J. E. Anthony, Appl. Phys. Lett. **94,** 013306 (2009).

[8] W. E. B. Shepherd, A. D. Platt, D. Hofer, O. Ostroverkhova, M. A. Loth, and J. E. Anthony, Appl. Phys. Lett. **97,** 163303 (2010).

[9] W. E. B. Shepherd, A. D. Platt, M. J. Kendrick, M. A. Loth, J. E. Anthony, and O. Ostroverkhova, J. Phys. Chem. Lett. **2,** 362 (2011).

[10] S. Subramanian, S. K. Park, S. R. Parkin, V. Podzorov, T. N. Jackson, and J. E. Anthony, J. Am. Chem. Soc. **130,** 2706 (2008).

[11] O. D. Jurchescu, D. A. Mourey, S. Subramanian, S. R. Parkin, B. M. Vogel, J. E. Anthony, T. N. Jackson, and D. J. Gundlach, Phys. Rev. B **80,** 085201 (2009).

[12] R. J. Kline, S. D. Hudson, X. Zhang, D. J. Gundlach, A. J. Moad, O. D. Jurchescu, T. N. Jackson, S. Subramanian, J. E. Anthony, M. F. Toney, and L. J. Richter, Chem. Mater. **23,** 1194 (2011).

[13] M. T. Lloyd, A. C. Mayer, S. Subramanian, D. A. Mourey, D. J. Herman, A. V. Bapat, J. E. Anthony, and G. G. Malliaras, J. Am. Chem. Soc. **129,** 9144 (2007).

[14] Z. Li, Y. F. Lim, J. Kim, S. R. Parkin, Y. L. Loo, G. G. Malliaras, and J. E. Anthony, Chem. Commun. **47,** 7617 (2011).

[15] J. Gao and F. A. Hegmann, Appl. Phys. Lett. **93,** 223306 (2008).

[16] K. Walzer, B. Maennig, M. Pfeiffer, and K. Leo, Chem. Rev. **107,** 1233 (2007).

[17] I. D. W. Samuel and G. A. Turnbull, Chem. Rev. **107,** 1272 (2007).

[18] O. D. Jurchescu, S. Subramanian, R. J. Kline, S. D. Hudson, J. E. Anthony, T. N. Jackson, and D. J. Gundlach, Chem. Mater. **20,** 6733 (2008).

[19] M. T. Lloyd, Y. F. Lim, and G. G. Malliaras, Appl. Phys. Lett. **92,** 143308 (2008).

[20] Supporting information can be found in the EPAPS Document No.xxx. For more information on EPAPS, see http://www.aip.org/pubservs/ epaps.html.

[21] V. Coropceanu, J. Cornil, D. da Silva, Y. Olivier, R. J. Silbey, and J. L. Bredas, Chem. Rev. **107,** 926 (2007).

[22] J. Day, A. D. Platt, S. Subramanian, J. E. Anthony, and O. Ostroverkhova, J. Appl. Phys. **105,** 103703 (2009).

[23] W. E. B. Shepherd, A. D. Platt, G. Banton, D. Hofer, M. A. Loth, J. E. Anthony, and O. Ostroverkhova, Proc. of SPIE **7935,** 79350G (2011).

[24] W. E. B. Shepherd, A. D. Platt, G. Banton, M. A. Loth, J. E. Anthony, and O. Ostroverkhova, Proc. of SPIE **7599,** 7599R (2010).

[25] A. D. Platt, J. Day, W. E. B. Shepherd, and O. Ostroverkhova, in *Organic Thin Films for Photonic Applications*; *Vol. 1039*, edited by S. H. Foulger (ACS Symposium Series, Washington, D.C., 2010), p. 211.

[26] S. Guha, J. D. Rice, Y. T. Yau, C. M. Martin, M. Chandrasekhar, H. R. Chandrasekhar, R. Guentner, P. Scanduicci de Freitas, and U. Scherf, Phys. Rev. B **67,** 125204 (2003).

[27] O. Ostroverkhova, S. Shcherbyna, D. G. Cooke, R. F. Egerton, F. A. Hegmann, R. R. Tykwinski, S. R. Parkin, and J. E. Anthony, J. Appl. Phys. **98,** 033701 (2005).

[28] F. C. Spano, J. Chem. Phys. **122,** 234701 (2005).

[29] F. C. Spano, Acc. Chem. Res. **43,** 429 (2010).

[30] F. C. Spano, J. Clark, C. Silva, and R. H. Friend, J. Chem. Phys. **130,** 074904 (2009).

[31] O. Kwon, V. Coropceanu, N. E. Gruhn, J. C. Durivage, J. G. Laquindanum, H. E. Katz, J. Cornil, and J. L. Bredas, J. Chem. Phys. **120,** 8186 (2004).

[32] C. C. Wu, E. Ehrenfreund, J. J. Gutierrez, J. P. Ferraris, and Z. V. Vardeny, Phys. Rev. B **71,** 081201(R) (2005).

[33] H. Sun, Z. Zhao, F. C. Spano, D. Beljonne, J. Cornil, Z. Shuai, and J. L. Bredas, Adv. Mat. **15,** 818 (2003).

[34] A. Y. Kobitski, R. Scholz, D. R. T. Zahn, and H. P. Wagner, Phys. Rev. B **68,** 155201 (2003).

[35] M. Kytka, L. Gisslen, A. Gerlach, U. Heinemeyer, J. Kovac, R. Scholz, and F. Schreiber, J. Chem. Phys. **130,** 214507 (2009).

[36] P. Pingel, A. Zen, R. D. Abellon, F. C. Grozema, L. D. A. Siebbeles, and D. Neher, Adv. Funct. Mater. **20,** 2286 (2010).

[37] S. C. J. Meskers, R. A. J. Janssen, J. E. M. Haverkort, and J. H. Wolter, Chem. Phys. **260,** 415 (2000).

[38] J. Clark, J. F. Chang, F. C. Spano, R. H. Friend, and C. Silva, Appl. Phys. Lett. **94,** 163306 (2009).

[39] J. F. Chang, J. Clark, N. Zhao, H. Sirringhaus, D. W. Breiby, J. W. Andreasen, M. M. Nielsen, M. Giles, M. Heeney, and I. McCulloch, Phys. Rev. B **74,** 115318 (2006).

[40] A. Salleo, R. J. Kline, D. M. DeLongchamp, and M. L. Chabinyc, Adv. Mat. **22,** 3812 (2010).

[41] J. Knoester, J. Chem. Phys. **99,** 8466 (1993).

[42] J. Clark, C. Silva, R. H. Friend, and F. C. Spano, Phys. Rev. Lett. **98,** 206406 (2007).

[43] A. Troisi and D. L. Cheung, J. Chem. Phys. **131,** 014703 (2009).

[44] A. Troisi, G. Orlandi, and J. E. Anthony, Chem Mater **17,** 5024 (2005).

[45] R. S. Sanchez-Carrera, P. Paramonov, G. M. Day, V. Coropceanu, and J. L. Bredas, J. Am. Chem. Soc. **132,** 14437 (2010).

[46] S. Ciuchi and S. Fratini, Phys. Rev. Lett. **106,** 166403 (2011).

[47] L. Raimondo, M. Laicini, P. Spearman, S. Tavazzi, and A. Borghesi, J. Chem. Phys. **125,** 024702 (2006).

[48] L. Wang, Q. Li, Z. Shuai, L. Chen, and Q. Shi, Phys. Chem. Chem. Phys. **12,** 3309 (2010).

[49] N. S. Sariciftci, *Primary Photoexcitations in Conjugated Polymers: Molecular Exciton versus Semiconductor Band Model* (World Scientific, Singapore, 1997).

[50] C. Deibel and V. Dyakonov, Rep. Prog. Phys. **73,** 096401 (2010).

[51] Y. Luo, H. Aziz, R. Klenkler, G. Xu, and Z. D. Popovic, Chem. Phys. Lett. **458,** 319 (2008).

[52] G. Gigli, F. Della Sala, M. Lomascolo, M. Anni, G. Barbarella, A. Di Carlo, P. Lugli, and R. Cingolani, Phys. Rev. Lett. **86,** 167 (2001).

[53] U. Rauscher, H. Bassler, D. D. C. Bradley, and M. Hennecke, Phys. Rev. B **42,** 9830 (1990).

[54] M. Bednarz, V. A. Malyshev, and J. Knoester, J. Chem. Phys. **117,** 6200 (2002).

[55] M. Bednarz, V. A. Malyshev, and J. Knoester, J. Chem. Phys. **120,** 3827 (2004).

[56] E. Da Como, M. A. Loi, M. Murgia, R. Zamboni, and M. Muccini, J. Am. Chem. Soc. **128,** 4277 (2006).

[57] Z. D. Popovic, M. I. Khan, A. M. Hor, J. L. Goodman, and J. F. Graham, J. Phys. Chem. B **106,** 8625 (2002).

[58] Z. D. Popovic, M. I. Khan, S. J. Atherton, A. M. Hor, and J. L. Goodman, J. Phys. Chem. B **102,** 657 (1998).

[59] V. I. Arkhipov and H. Bassler, Phys. Stat. Sol. A **6,** 1152 (2004).

[60] D. Hertel, E. V. Soh, H. Bassler, and L. J. Rothberg, Chem. Phys. Lett. **361,** 99 (2002).

[61] M. C. J. M. Vissenberg and M. J. M. de Jong, Phys. Rev. B **57,** 2667 (1998).

[62] H. Najafov, I. Biaggio, T. K. Chuang, and M. K. Hatalis, Phys. Rev. B **73,** 125202 (2006).

[63] D. Moses, J. Wang, A. J. Heeger, N. Kirova, and S. Brazovski, P. Natl .Acad. Sci. USA **98,** 13496 (2001).

[64] A. Haugeneder, U. Lemmer, and U. Scherf, Chem. Phys. Lett. **351,** 354 (2002).

[65] O. Ostroverkhova, D. G. Cooke, S. Shcherbyna, R. F. Egerton, F. A. Hegmann, R. R. Tykwinski, and J. E. Anthony, Phys. Rev. B **71,** 035204 (2005).

[66] D. Moses, C. Soci, X. Chi, and A. P. Ramirez, Phys. Rev. Lett. **97,** 067401 (2006).

[67] D. Moses, A. Dogariu, and A. J. Heeger, Phys. Rev. B **61,** 9373 (2000).

[68] D. Moses, M. Sinclair, and A. J. Heeger, Phys. Rev. Lett. **58,** 2710 (1987).

[69] H. Y. Liang, W. L. Cao, M. Du, Y. Kim, W. N. Herman, and C. H. Lee, Chem. Phys. Lett. **419,** 292 (2006).

[70] D. Moses, H. Okumoto, C. H. Lee, A. J. Heeger, T. Ohnishi, and T. Noguchi, Phys. Rev. B **54,** 4748 (1996).

[71] P. W. M. Blom, M. J. M. De Jong, and M. G. van Munster, Phys. Rev. B **55,** R656 (1997).

[72] A. Pivrikas, M. Ullah, H. Sitter, and N. S. Sariciftci, Appl. Phys. Lett. **98,** 092114 (2011).

[73] D. Hertel and H. Bassler, Chemphyschem **9,** 666 (2008).

[74] F. A. Hegmann, R. R. Tykwinski, K. P. H. Lui, J. E. Bullock, and J. E. Anthony, Phys. Rev. Lett. **89,** 227403 (2002).

[75] N. Christ, S. W. Kettlitz, S. Zufle, S. Valouch, and U. Lemmer, Phys. Rev. B **83,** 195211 (2011).

[76] R. A. Street, K. W. Song, J. E. Northrup, and S. Cowan, Phys. Rev. B **83,** 165207 (2011).

[77] R. Konenkamp, G. Priebe, and B. Pietzak, Phys. Rev. B **60,** 11804 (1999).

[78] S. Etemad, T. Mitani, M. Ozaki, T. C. Chung, A. J. Heeger, and A. G. MacDiarmid, Sol. Stat. Commun. **40,** 75 (1981).

[79] E. A. Silinsh and V. Capec, *Organic molecular crystals: interaction, localization and transport phenomena* (American Institute of Physics, New York, 1994).

[80] C. H. Lee, G. Yu, D. Moses, K. Pakbaz, C. Zhang, N. S. Sariciftci, A. J. Heeger, and F. Wudl, Phys. Rev. B **48,** 15425 (1993).

[81] L. Smilowitz, N. S. Sariciftci, R. Wu, C. Gettinger, A. J. Heeger, and F. Wudl, Phys. Rev. B **47,** 13835 (1993).

[82] A. Haugeneder, M. Neges, C. Kallinger, W. Spirkl, U. Lemmer, J. Feldmann, U. Scherf, E. Harth, A. Gugel, and K. Mullen, Phys. Rev. B **59,** 15346 (1999).

[83] O. Ostroverkhova, D. G. Cooke, F. A. Hegmann, J. E. Anthony, V. Podzorov, M. E. Gershenson, O. D. Jurchescu, and T. T. M. Palstra, Appl. Phys. Lett. **88,** 162101 (2006).

[84] P. B. Miranda, D. Moses, and A. J. Heeger, Phys. Rev. B **64,** 081202(R) (2001).

[85] V. I. Arkhipov, E. V. Emelianova, and H. Bassler, Phys. Rev. Lett. **82,** 1321 (1999).

[86] W. Barford, J. Chem. Phys. **126,** 134905 (2007).

[87] J. Cornil, D. A. Dos Santos, X. Crispin, R. J. Silbey, and J. L. Bredas, J. Am. Chem. Soc. **120,** 1289 (1998).

[88] Z. Shuai, L. Wang, and Q. Li, Advanced Materials **23,** 1145 (2011).

[89] J. F. Chang, H. Sirringhaus, M. Giles, M. Heeney, and I. McCulloch, Phys. Rev. B **76,** 205204 (2007).

[90] N. S. Ginsberg, Y. C. Cheng, and G. R. Fleming, Accounts of Chemical Research **42,** 1352 (2009).

[91] S. Tao, H. Matsuzaki, H. Uemura, H. Yada, T. Uemura, J. Takeya, T. Hasegawa, and H. Okamoto, Phys. Rev. B **83,** 075204 (2011).

Figure captions

Figure 1. Molecular structures (a) and HOMO, LUMO energy levels (b). R = TES or TIPS, R' = F or CN.

Figure 2. (a) Optical absorption spectra of a pristine ADT-TES-F film at several temperatures. The arrow shows the position of the 0-0 absorption peak of ADT-TES-F molecules in toluene solution.

(b) Peak positions of absorption bands A_1 and A_2 (corresponding to absorptive 0-0 and 0-1 transitions), as well as of PL bands 1 and 2 (corresponding to emissive 0-0 and 0-1 transitions). Linear fits, with parameters listed in the text, are also shown. Gaussian widths σ_{abs} and σ_{PL} of the absorption and PL lines are included as error bars. The PL 0-0 peak position at 100 K corresponds to the Stokes shift of $2.85\sigma_{abs}$. Calculated PL 0-0 peak positions due to Stokes shifts equal to $\sigma_{abs}^2/(k_BT)$ are indicated by stars.

Figure 3. (a) PL spectra of a pristine ADT-TES-F film at several temperatures. PL bands 1-3, corresponding to 0-n transitions (with n = 0, 1, 2) are indicated. Inset shows selected spectra normalized at the peak value of the PL band 2. (b) Integrated PL intensities $I_{0\text{-}n}$ (with n = 0, 1, 2), normalized at their respective values at 100 K, as functions of temperature. Inset shows Arrhenius fits of the normalized integrated intensity of the PL band 2 ($I_{0\text{-}1}$) and the $I_{0\text{-}0}/I_{0\text{-}1}$ ratio with Δ_{PL} = 0.069±0.003 eV and Δ = 0.063±0.003 eV, respectively.

Figure 4. PL lifetimes τ_1, τ_2 (a) and their corresponding amplitudes a_1, a_2 (b) obtained from bi-exponential fits of the PL decays in pristine ADT-TES-F films. Dashed lines are guides for the eye. Also shown in (a) are average time constant τ_{av} calculated as described

in text, as well as PL lifetimes τ_1, τ_2 of the PL band 1 (0-0 transition). Dash-dotted line in (a) represents the radiative lifetime of ADT-TES-F isolated molecules.

Figure 5. PL spectra of a pristine ADT-TES-F film at 190 K, at various applied electric fields (shown on the left, in units of V/cm). Inset shows the electric field-induced PL quenching parameter Q of Eq.(3) as a function of applied electric field at various temperatures. Fit of the data at 100 K to Eq.(4) and the binding energy E_b = 0.097±0.003 eV are also included.

Figure 6. (a) Transient photocurrent obtained under 355 nm 500 ps photoexcitation of a pristine ADT-TES-F film at 1.2×10^5 V/cm, at various temperatures. Inset shows photocurrent transients measured at 298 K and 98 K, normalized by their peak values. (b) Electric field dependence of the product of the charge carrier mobility μ and photogeneration efficiency η at various temperatures. Fits with the Poole-Frenkel model ($\mu\eta \sim \exp(\gamma\sqrt{E})$) are also included. Inset shows the fit parameter γ as a function of inverse temperature, fit with Eq.(6).

Figure 7. Temperature dependence of the peak photocurrent $I_{ph,peak}$ normalized by its value at 300 K obtained in a pristine ADT-TES-F film and ADT-TES-F/C_{60} (2%) and ADT-TES-F/ADT-TIPS-CN (2%) composites at 1.2×10^5 V/cm. The dashed line is a guide for the eye. Inset shows a fit of the data with $I_{ph,peak} \sim \exp(-\Delta_{ph}/k_BT)$ for a pristine ADT-TES-F film with activation energy Δ_{ph} = 0.025±0.003 eV.

Figure 8. Transient photocurrent measured under 355 nm 500 ps photoexcitation in an ADT-TES-F/C_{60} film at 1.2 x 10^5 V/cm, at various temperatures. Inset shows photocurrent transients measured at 298 K and 98 K, normalized by their peak values.

Figure 9. (a) PL spectra obtained from an ADT-TES-F/ADT-TIPS-CN film at various temperatures. Left inset: inverse of PL QY, normalized by its value at 100 K, as a function of inverse temperature, fit with $I_{PL} \sim \exp(-\Delta_{PL}/k_BT)$ at $\Delta_{PL} = 0.08 \pm 0.02$ eV. Right inset: electric field-induced PL quenching parameter Q as a function of applied electric field, at 98 K and 352 K. A fit of the data at 98 K to Eq.(4) and the binding energy $E_b = 0.045 \pm 0.003$ eV are also included.

(b) and (c): PL lifetimes τ_1, τ_2 (b) and their corresponding amplitudes a_1, a_2 (c) obtained from bi-exponential fits of the PL decays in ADT-TES-F/ADT-TIPS-CN films. The average time constant τ_{av} (calculated as described in text) is also shown. Dashed lines are guides for the eye.

Figure 10. Transient photocurrent measured under 355 nm 500 ps photoexcitation in an ADT-TES-F/ADT-TIPS-CN film at 1.2×10^5 V/cm, at various temperatures.

Figure 11. Schematics of exciton and charge carrier dynamics in pristine ADT-TES-F and ADT-TES-F-based composite films. The ground state and first two excited vibronic levels, separated by the effective vibronic frequency ω_{eff}, are shown for ADT-TES-F. The photoexcitation of ADT-TES-F with ω_{ex} is distributed among charge carrier photogeneration (η), emissive exciton formation, and other possible channels. The part of the excitation responsible for PL emission rapidly relaxes to a vibronically relaxed electronic excited state S_1, from which the exciton recombines either radiatively or nonradiatively, depending on the temperature and electric field. The oscillator strength increases towards the top of the exciton band, as the 0-0 emission becomes more allowed. Small black crosses indicate dark states. Symbols in red indicate processes that are either

disabled (crosses: thermally activated nonradiative recombination; dashed-line crosses indicate slow nonradiative recombination processes, occurring on nanosecond time scales, whereas solid-line crosses represent faster, sub-200 ps, processes) or enabled (arrows: electric field-activated nonradiative recombination) at low temperatures. Upon the addition of C_{60} to the ADT-TES-F host, fast photoinduced electron transfer (k_{ET}) occurs from ADT-TES-F to C_{60}, resulting in improved charge carrier photogeneration (η). Upon the addition of ADT-TIPS-CN, the exciplex forms between the ADT-TES-F and ADT-TIPS-CN (k_{exci}) with the relaxed ADT-TES-F exciton acting as a precursor. The exciplex decays radiatively with a lifetime τ_{exci}, has a slow nonradiative recombination channel (dashed-line cross), and can dissociate into free charge carriers (η_{exci}) under applied electric field at room temperature.

Figure 1

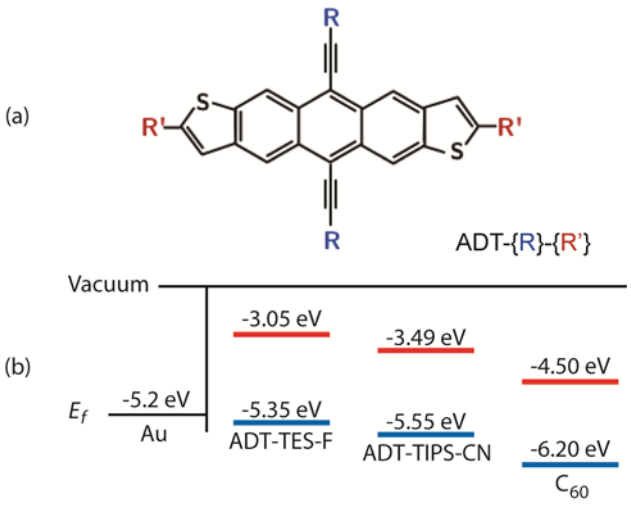
(a)
R
R'
S
S
R'
R
ADT-{R}-{R'}
(b)
Vacuum
-3.05 eV
-3.49 eV
-4.50 eV
E_f
-5.2 eV
Au
-5.35 eV
ADT-TES-F
-5.55 eV
ADT-TIPS-CN
-6.20 eV
C_{60}

Figure 2

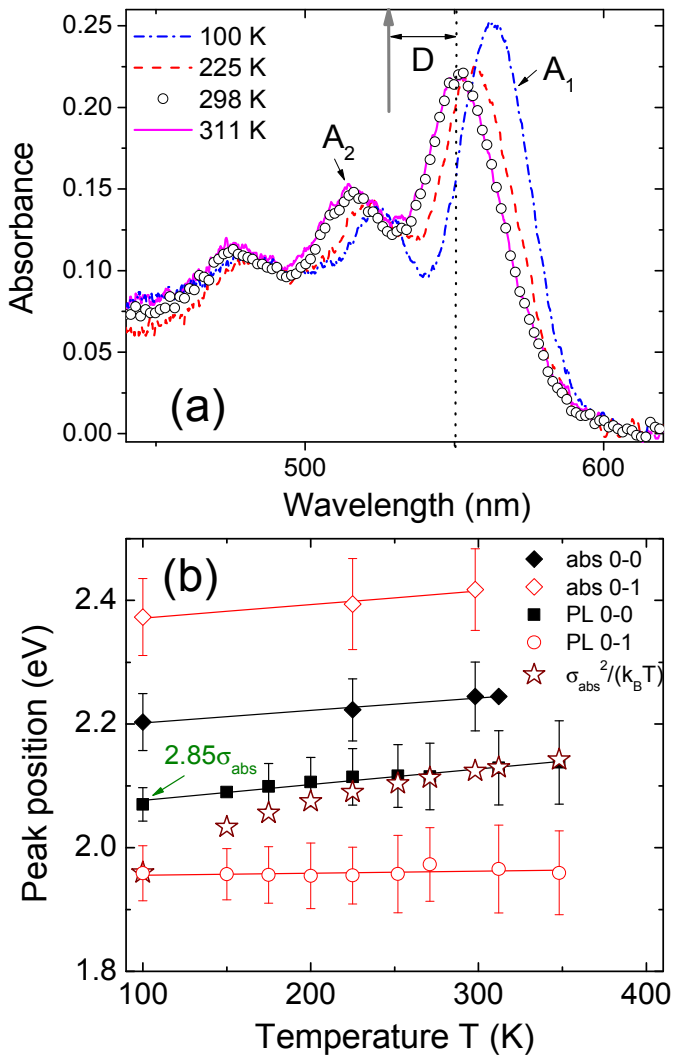
100 K
225 K
298 K
311 K
D
A1
A2
(a)
Absorbance
Wavelength (nm)
0.25
0.20
0.15
0.10
0.05
0.00
500
600
(b)
abs 0-0
abs 0-1
PL 0-0
PL 0-1
σabs²/(kBT)
2.85σabs
Peak position (eV)
Temperature T (K)
2.4
2.2
2.0
1.8
100
200
300
400

Figure 3

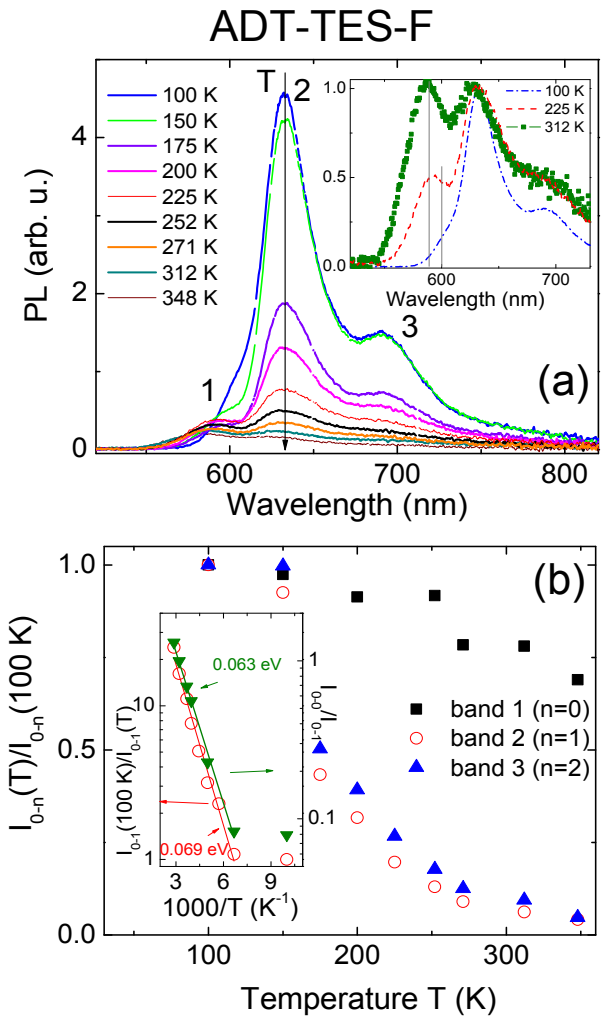
ADT-TES-F
100 K
150 K
175 K
200 K
225 K
252 K
271 K
312 K
348 K
T
1
2
3
(a)
PL (arb. u.)
Wavelength (nm)
100 K
225 K
312 K
(b)
band 1 (n=0)
band 2 (n=1)
band 3 (n=2)
0.063 eV
0.069 eV
1000/T (K-1)
Temperature T (K)

Figure 4

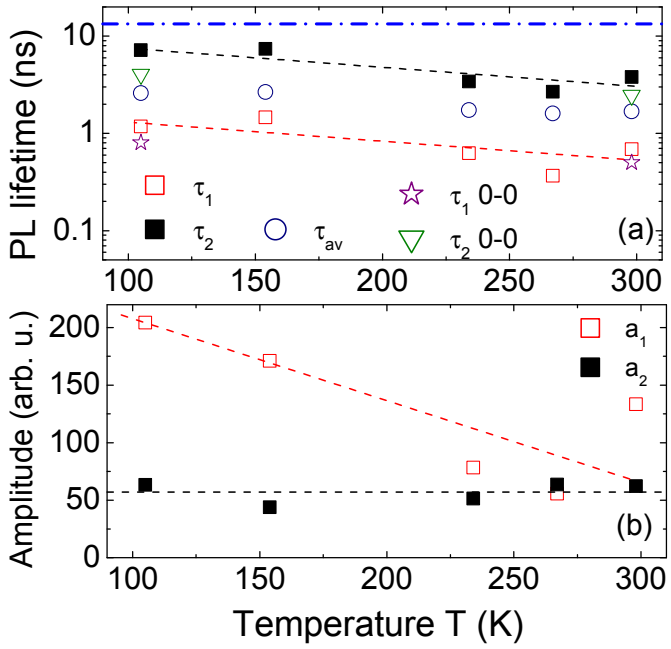
PL lifetime (ns)
10
1
0.1
100
150
200
250
300
τ1
τ2
τav
τ1 0-0
τ2 0-0
(a)
Amplitude (arb. u.)
200
150
100
50
0
a1
a2
(b)
Temperature T (K)

Figure 5

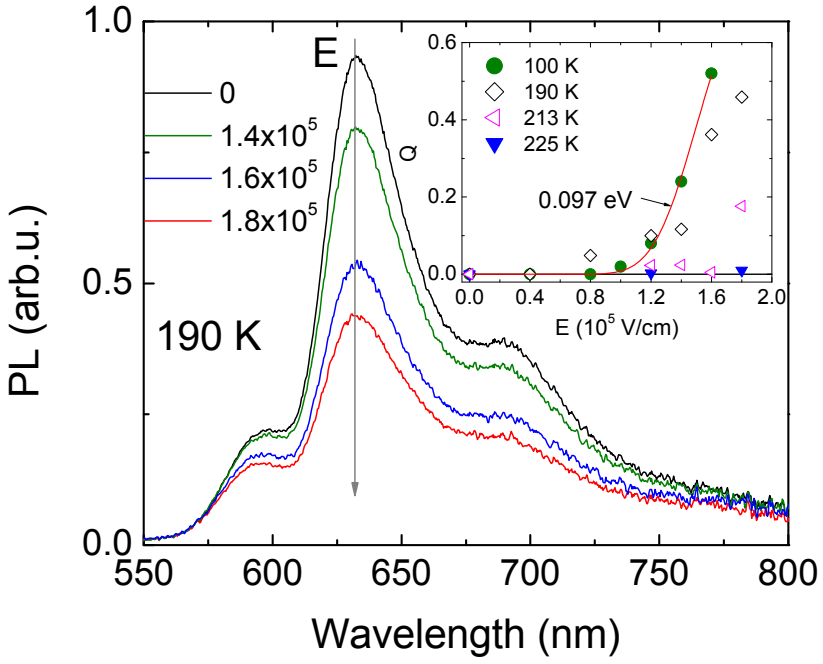
1.0
0.5
0.0
PL (arb.u.)
550
600
650
700
750
800
Wavelength (nm)
E
0
1.4x10^5
1.6x10^5
1.8x10^5
190 K
Q
0.6
0.4
0.2
0.0
100 K
190 K
213 K
225 K
0.097 eV
0.0
0.4
0.8
1.2
1.6
2.0
E (10^5 V/cm)

Figure 6

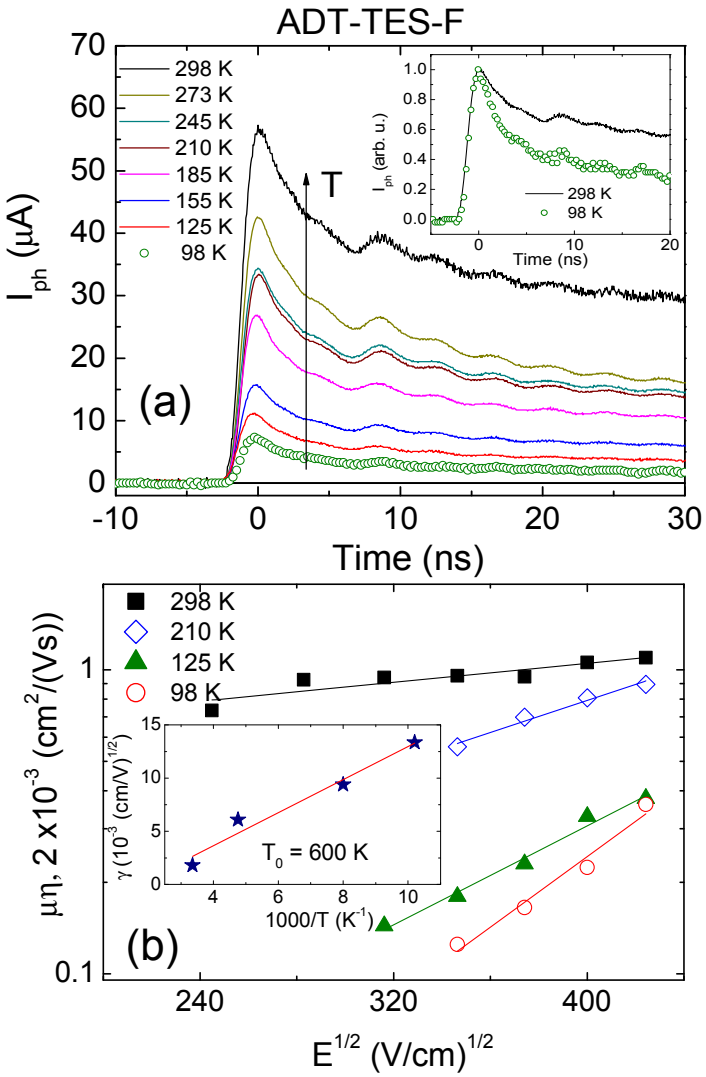
ADT-TES-F
298 K
273 K
245 K
210 K
185 K
155 K
125 K
98 K
T
(a)
I_{ph} (μA)
Time (ns)
I_{ph} (arb. u.)
298 K
98 K
Time (ns)
298 K
210 K
125 K
98 K
T_0 = 600 K
γ (10^{-3} (cm/V)$^{1/2}$)
1000/T (K^{-1})
(b)
μη, 2 x10^{-3} (cm^2/(Vs))
$E^{1/2}$ (V/cm)$^{1/2}$

Figure 7

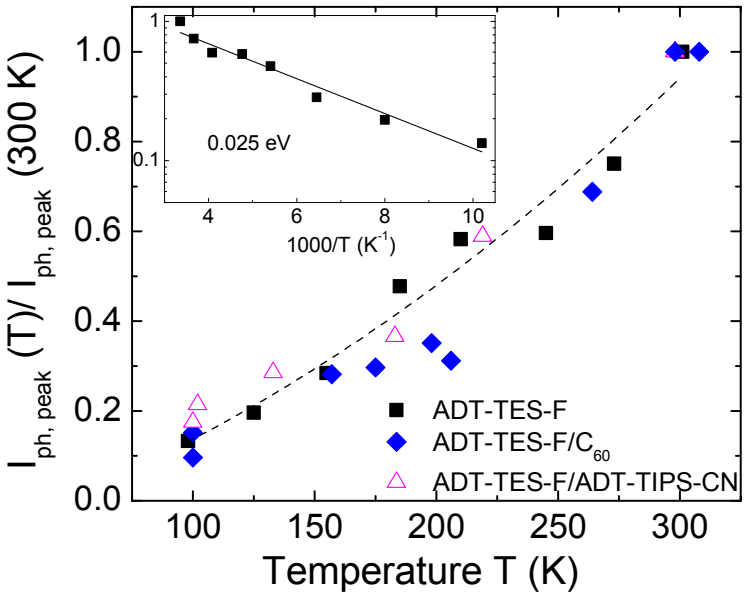
1.0
0.8
0.6
0.4
0.2
0.0
100
150
200
250
300
Temperature T (K)
$I_{ph, peak}$ (T)/ $I_{ph, peak}$ (300 K)
ADT-TES-F
ADT-TES-F/C_{60}
ADT-TES-F/ADT-TIPS-CN
1
0.1
0.025 eV
4
6
8
10
1000/T (K^{-1})

Figure 8

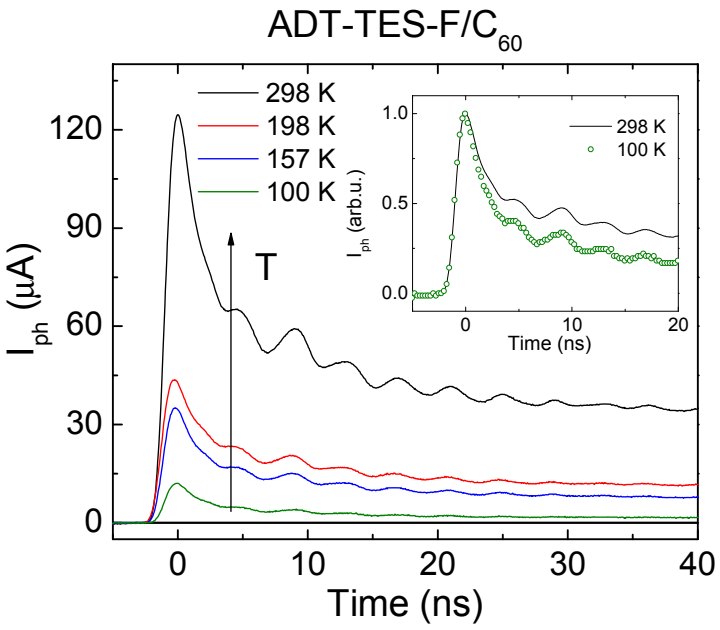
ADT-TES-F/C60
298 K
198 K
157 K
100 K
T
Iph (μA)
Time (ns)
298 K
100 K
Iph (arb.u.)
Time (ns)

Figure 9

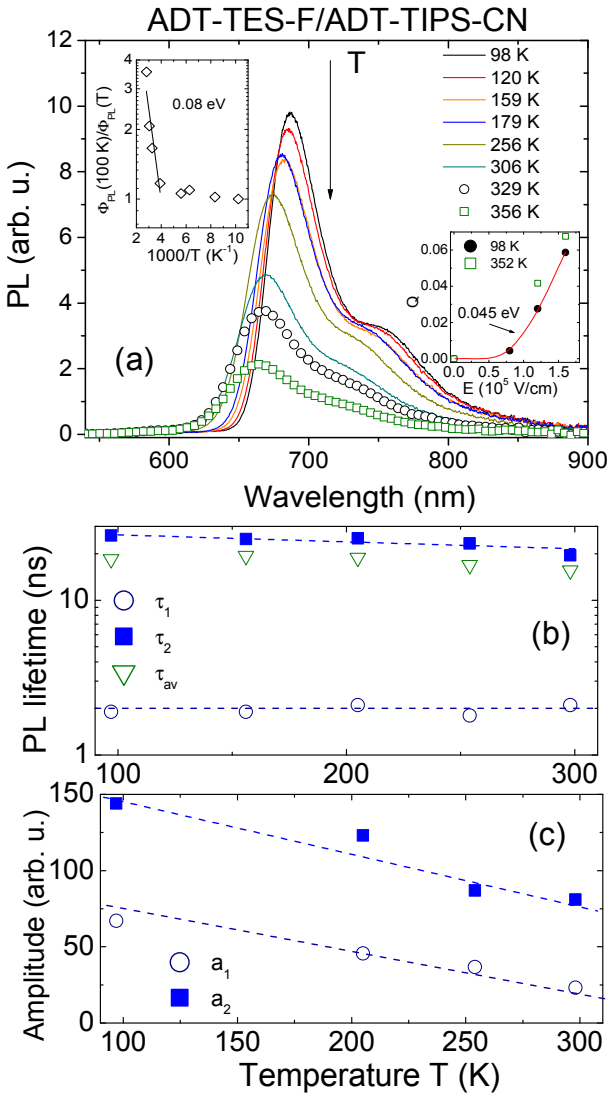
ADT-TES-F/ADT-TIPS-CN
PL (arb. u.)
Wavelength (nm)
T
98 K
120 K
159 K
179 K
256 K
306 K
329 K
356 K
(a)
0.08 eV
1000/T (K-1)
98 K
352 K
0.045 eV
E (10^5 V/cm)
PL lifetime (ns)
τ1
τ2
τav
(b)
Amplitude (arb. u.)
a1
a2
(c)
Temperature T (K)

Figure 10

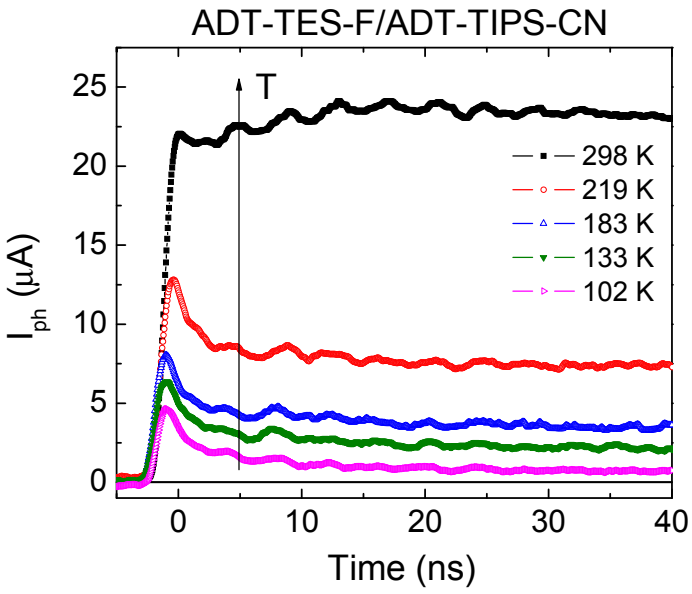
ADT-TES-F/ADT-TIPS-CN
T
298 K
219 K
183 K
133 K
102 K
I_{ph} (μA)
Time (ns)
0
5
10
15
20
25
0
10
20
30
40

Figure 11

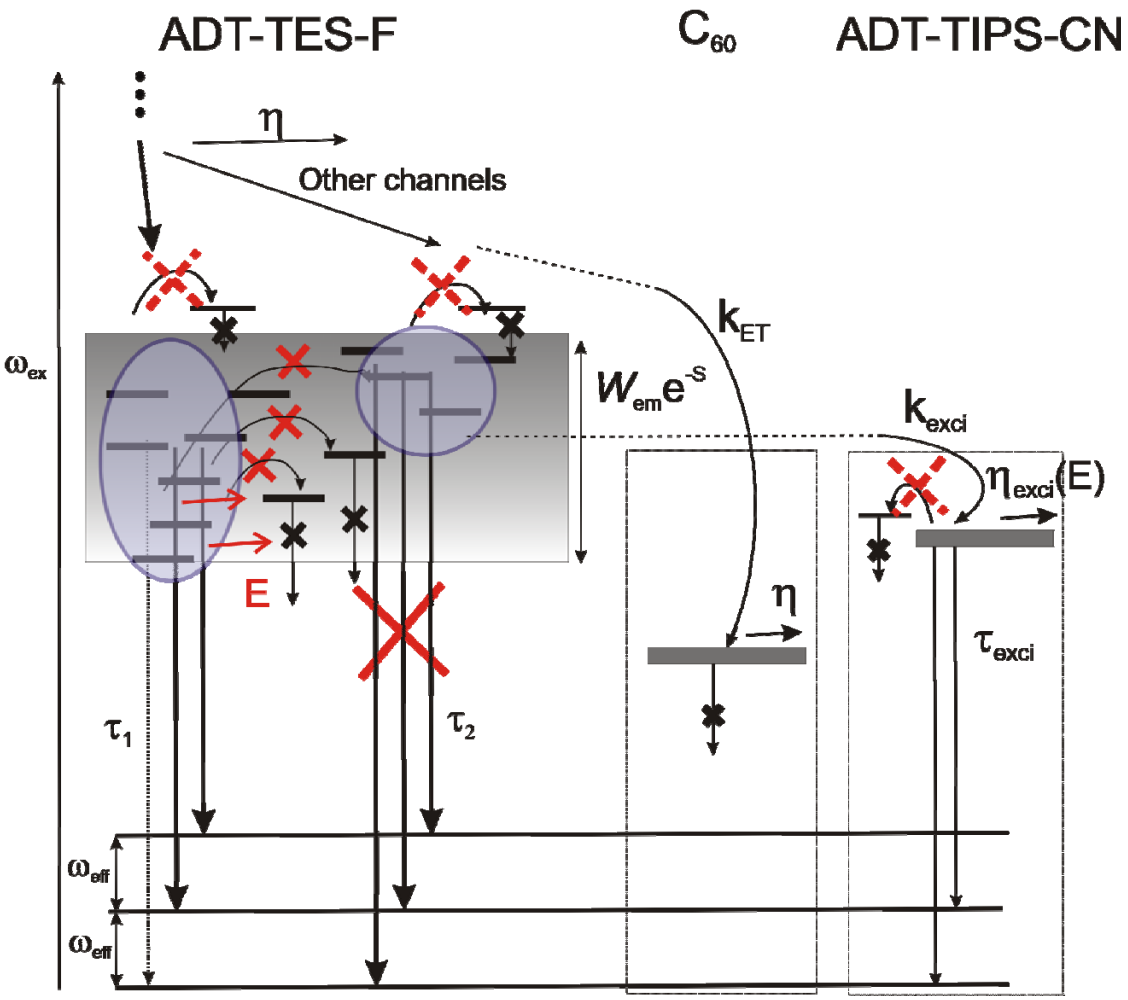
ADT-TES-F
C60
ADT-TIPS-CN
η
Other channels
kET
ωex
Wem e-s
kexci
ηexci(E)
E
η
τexci
τ1
τ2
ωeff
ωeff